

Fall 1994

Implementation of time-frequency distribution software and its use to study biological signals

Mansour Adib

New Jersey Institute of Technology

Follow this and additional works at: <https://digitalcommons.njit.edu/theses>



Part of the [Electrical and Electronics Commons](#)

Recommended Citation

Adib, Mansour, "Implementation of time-frequency distribution software and its use to study biological signals" (1994). *Theses*. 1162.
<https://digitalcommons.njit.edu/theses/1162>

This Thesis is brought to you for free and open access by the Theses and Dissertations at Digital Commons @ NJIT. It has been accepted for inclusion in Theses by an authorized administrator of Digital Commons @ NJIT. For more information, please contact digitalcommons@njit.edu.

Copyright Warning & Restrictions

The copyright law of the United States (Title 17, United States Code) governs the making of photocopies or other reproductions of copyrighted material.

Under certain conditions specified in the law, libraries and archives are authorized to furnish a photocopy or other reproduction. One of these specified conditions is that the photocopy or reproduction is not to be “used for any purpose other than private study, scholarship, or research.” If a user makes a request for, or later uses, a photocopy or reproduction for purposes in excess of “fair use” that user may be liable for copyright infringement,

This institution reserves the right to refuse to accept a copying order if, in its judgment, fulfillment of the order would involve violation of copyright law.

Please Note: The author retains the copyright while the New Jersey Institute of Technology reserves the right to distribute this thesis or dissertation

Printing note: If you do not wish to print this page, then select “Pages from: first page # to: last page #” on the print dialog screen

The Van Houten library has removed some of the personal information and all signatures from the approval page and biographical sketches of theses and dissertations in order to protect the identity of NJIT graduates and faculty.

ABSTRACT

IMPLEMENTATION OF TIME-FREQUENCY DISTRIBUTION SOFTWARE AND ITS USE TO STUDY BIOLOGICAL SIGNALS

by
Mansour Adib

The joint time-frequency signal representation has received considerable attention as a powerful tool for analyzing biological signals. It combine time-domain and frequency-domain analyses to yield a potentially more revealing picture of the temporal localization of a signal's spectral components. In this research we have developed algorithm which implement time-frequency signal analysis techniques on a computer system. Its primary function is to produce a variety of time-frequency representations and plots from the time series. Numerous generated signals were used to justify our computer algorithm.

Variety of time-frequency distribution were utilized to expand the concept of spectral analysis of heart rate variability, to describe changes in vagal tone and sympatho-vagal balance as a function of time. As a result the assessment of the autonomic nervous system during rapid changes in heart rate was made.

The smoothed Pseudo Wigner distribution was applied to electromyographic(EMG) signal during muscle fatigue. The mesh plot of the time-frequency analysis showed, the median frequency of the EMG decline during muscle fatigue.

**IMPLEMENTATION OF TIME-FREQUENCY DISTRIBUTION SOFTWARE
AND ITS USE TO STUDY BIOLOGICAL SIGNALS**

by
Mansour Adib

**A Thesis
Submitted to the Faculty of
New Jersey Institute of Technology
in Partial Fulfillment of the Requirements for the Degree of
Master of Science in Electrical Engineering**

Department of Electrical and Computer Engineering

January 1995

APPROVAL PAGE

IMPLEMENTATION OF TIME-FREQUENCY DISTRIBUTION SOFTWARE
AND ITS USE TO STUDY BIOLOGICAL SIGNALS

Mansour Adib

Dr. Stanley S. Reisman, Thesis Advisor Date
Professor of Electrical Engineering and Associate
Chairperson for Graduate Studies, NJIT

Dr. Peter Engler, Committee Member Date
Associate Professor of Electrical Engineering, NJIT

Dr. Thomas W. Findley, Committee Member Date
Associate Professor of Medicine, UMDNJ
Director of Research, Kessler Institute for
Rehabilitation

BIOGRAPHICAL SKETCH

Author: Mansour Adib

Degree: Master of Science in Electrical Engineering

Date: January 1995

Undergraduate and Graduate Education:

- Master of Science in Electrical Engineering
New Jersey Institute of Technology, Newark, NJ, 1995
- Bachelor of Science in Electrical Engineering
New Jersey Institute of Technology, Newark, NJ, 1992

Major: Electrical Engineering

This thesis is dedicated to my parents,
Akram and Reza Adib.

ACKNOWLEDGMENT

The author wishes to express his sincere appreciation to his advisor, Dr. Stanley S. Reisman, for his supervision, affiliation and moral sense throughout this research.

Special thanks to Drs. Peter Engler and Thomas W. Findley for serving as members of the committee.

Special acknowledgment is due to John Andrews, who influenced some of the software routines in this research.

TABLE OF CONTENTS

Chapter	Page
1 INTRODUCTION	1
1.1 Scope of Thesis	1
1.2 Time and Frequency Analysis	2
1.3 Properties of Joint Time-Frequency Distributions.....	4
1.4 Joint Time-Frequency Analysis Illustration.....	7
2 CATEGORIZATION OF TIME-FREQUENCY DISTRIBUTIONS	10
2.1 Linear Time-Frequency Distribution	10
2.2 Bilinear Time-Frequency Distribution.....	10
2.3 Analytic Signal.....	13
2.4 General Class of Time-Frequency Distribution	16
2.5 Kernel Function	16
2.5.1 Properties.....	17
2.6 Ambiguity Function Relationship.....	23
3 COMPARISON OF TIME-FREQUENCY DISTRIBUTIONS	26
3.1 Short Time Fourier Transform (Spectrogram).....	26
3.2 Wigner distribution	30
3.2.1 Windowed Wigner Distribution	36
3.3 The Exponential Distribution.....	37
3.4 Reduced Interference Distribution	40

TABLE OF CONTENTS
(continued)

Chapter	Page
3.5 Implementation of Algorithm using Matlab Software.....	43
3.5.1 Analytic Signal Calculation.....	45
3.6 General Approach to Computation of TFDs.....	46
3.7 Code fragments to generate $G(n,m)$	47
3.8 Optimization of Algorithm Using Matlab Software	47
4 APPLICATION OF TIME FREQUENCY DISTRIBUTION	52
4.1 Autonomic Nervous System	52
4.1.1 Protocol and Acquisition of InterBeat Interval.....	54
4.1.2 Vagal Tone and Sympatho-Vagal Balance via Time-Frequency Distribution during Exercise on a Bicycle	54
4.2 Physiology of Electromyographic Signal (EMG).....	61
4.2.1 Integrity of the EMG Signal	62
4.2.2 Data Acquisition	63
4.2.3 Electromyographic Signal (EMG) via Time-Frequency Distribution during Muscle Fatigue	64
5 CONCLUSIONS.....	72
5.1 Development of the Time-Frequency Signal Analysis Toolbox	72
5.2 Biomedical Application of Time-Frequency Distribution.....	73
5.2.1 Sympatho-vagal Balance	73
5.2.2 Time-Frequency Distribution of EMG Signal.....	74

TABLE OF CONTENTS
(continued)

Chapter	Page
APPENDIX A SOURCE CODE OF TEST SIGNAL GENERATION AND TFA PACKAGE.....	75
REFERENCES	87

LIST OF TABLES

Table	Page
1 Some Distributions and Their Kernel Requirements.....	18
2 Distribution Properties and Associated Kernel.....	24
3 Requirements on $h(t)$ and Their Counterparts.....	43
4 TFDs and Their Determining Function $G(n,m)$	48
5 Results from SPWD of EMG using Surface Electrode.....	68
6 Results from SPWD of EMG using Fine Wire Electrode.....	70
7 The Statistical Values from Maniar's Work.....	71

LIST OF FIGURES

Figure	Page
1 The plots of three finite duration signal. All signals contain same three frequencies (2 ,5 and 10 hertz) except, it occurs at different time.....	6
2 The plots of power spectrum for the three finite signal. The spectrum just tells us that frequencies existed at 2, 5 and 10 hertz.....	6
3 The contour plot of time frequency analysis of three finite duration signal.....	9
4 Energy density spectrum.....	15
5 Ambiguity function of two sinewave signals.....	25
5 Spectrogram of a signal which consists of two components.....	29
7 Arbitrary finite signal.....	33
8 Arbitrary finite signal.....	34
9 The Wigner distribution of the sum of two infinite duration sine waves. The oscillating term in the middle of the two frequencies is the cross term.....	35
10 Performance of the Choi Williams distribution upon three cases with a) $\sigma = 1000$ b) $\sigma = 50$ and c) $\sigma = 1$	39
11 The ambiguity domain kernel of RID.....	44
12 Applying PWD to IBI (non-detrended).....	55
13 Applying PWD to IBI.....	56
14 Applying SPWD to IBI.....	57

LIST OF FIGURES
(Continued)

Figure	Page
15 Applying CWD to IBI.....	58
16 Applying BJD to IBI.....	59
17 Applying RMD to IBI.....	60
18 The mesh plot of EMG signal during muscle fatigue.....	65
19 The plot from the EMG signal using surface electrode.....	66
20 The plot from the EMG signal using surface electrode.....	67
21 The plot from the EMG signal using fine wire electrode.....	69
22 The plot from the EMG signal using fine wire electrode.....	76

CHAPTER 1

INTRODUCTION

Time-frequency signal representations characterize signals over a time-frequency plane. They combine time-domain and frequency-domain analyses to yield a potentially more revealing picture of the temporal localization of a signal's spectral components. In this research we have developed a time-frequency signal analysis toolbox. Its primary function is to produce a variety of time-frequency representations and plots from the time series, although it also has a number of auxiliary functions. Utilizing the time-frequency distribution, we compared median frequency and decline in median frequency of electromyography (EMG) signals during muscle fatigue with standard FFT spectral analysis methods. The time-frequency analysis was also used to compute the sympathetic and parasympathetic influence on heart rate variability. These applications will be further discussed in chapter 4.

1.1 Scope of Thesis

The aim of time-frequency analysis is to understand and develop the tools that can describe a time varying spectrum. The original computer algorithm(FORTRAN CODE) of time-frequency representation was presented by Boashash [1]. In this research we have regenerated his algorithm which implements time-frequency signal analysis techniques using Matlab software. Its primary function is to produce a variety of time-frequency

representations and plots from the time series. Currently, our time frequency analysis software includes the short time Fourier transform (STFT), The Pseudo Wigner distribution (PWD), The smoothed Pseudo Wigner distribution (SPWD), The Choi Williams distribution (CWD), The Born Jordan distribution (BJD) and The Rihaczek Margenau distribution (RMD). The most important feature of our software is its ease of extendibility for additional time-frequency distributions. Numerous generated signals were used to justify our computer algorithm.

In this research we have also applied our distributions to two types of biological signals. First, we used our distributions to better understand the information contained in an inter beat interval signal(heart rate variability). Expansion of the concept of spectral analysis into time-frequency analysis gave us the ability to observe how the parasympathetic and sympatho-vagal balance changed during rest, exercise and recovery.

Second, we applied the smoothed Pseudo Wigner distribution (SPWD) to compare median frequency and decline in median frequency of electromyography (EMG) signals during muscle fatigue with standard FFT spectral analysis methods. The time-frequency distribution result showed decline of median frequency during muscle fatigue. The correlation coefficient was shown to increase as the length of the analysis window was increased.

1.2 Time and Frequency Analysis

The study of a signal as a function of time is “ time analysis “. One of the most important ideas is how much energy is contained in signal $x(t)$ at time t . We define the energy

density to be $|x(t)|^2$. That is, in a small amount of time Δt , $|x(t)|^2 \Delta t$ represents the amount of energy in the signal[1].

However if we want to gain more understanding it is often better to study the signal in the “frequency domain”. One of the reasons for frequency analysis is that it simplifies our understanding of the wave forms which can be represented as simple sines , cosines and their sum. Hence if we have a complex signal but we realize that the signal is really the superposition of sine waves at fixed frequencies, the signal becomes simpler to understand and characterize. Another reason for frequency analysis is that in certain situations the propagation characteristics in a medium depend on the frequency, such as absorption of light by different materials[1].

Therefore we can expand the signal as

$$x(t) = \int_{-\infty}^{\infty} X(f) \cdot e^{j2\pi ft} df \quad (1.1)$$

and we can think of $X(f)$ as the signal in the frequency domain and the energy density per unit frequency is $|X(f)|^2$. That is, the fractional energy in the frequency interval Δf at frequency f is $|X(f)|^2 \Delta f$. Note that by inverting equation 1.1, we can define the signal in the frequency domain[1].

$$X(f) = \int_{-\infty}^{\infty} x(t) \cdot e^{-j2\pi ft} dt \quad (1.2)$$

$X(f)$ is referred to as the Fourier Transform of $x(t)$. Conversion back to the time domain is done using equation 1.1 and is referred to as the inverse Fourier transform of

$X(f)$.

The disadvantage of time and frequency analysis is that they do not fully describe what is happening. The Fourier transform tells us the frequencies that existed for the total duration of the signal, and not the frequencies which exist at a particular time.

In figure 1, we illustrate three cases, where each contains three sine waves of equal duration time of 2 seconds and frequencies of 2, 5 and 10 hertz. The only difference among cases “a”, “b” and “c” is that different frequencies occurs at different times. The power spectrum, as shown in figure 2, is the same for all three cases and shows that frequencies 2, 5 and 10 hertz were present for all cases but does not show when they existed. To fully describe such a situation we have to give the frequencies for each time.

1.3 Properties of Joint Time-Frequency Distributions

The method of musical notation is a time-frequency representation since it describes what frequency should be played as a function of time. In musical notation time is presented on the horizontal axis and the pitch on the vertical axis.

We want a joint distribution which will give us the fraction of the total energy of the signal at time t and frequency f . We call that distribution $\rho(t, f)$.

Note, when we say “A function represents the number of things per unit something”, that is called density. Hence joint time-frequency distribution $\rho(t, f)$ is really a joint time-frequency density function. To understand joint density functions, we briefly list some of its desirable properties. Define $x(t)$, $X(f)$, $\rho(t, f)$ as signal, Fourier transform of signal and joint time-frequency density respectively. Then;

1. Joint time-frequency density should be positive for all values of time and frequency because it indicates how much of the total energy is in a particular time-frequency cell.

That is ;

$$\rho(t, f) \geq 0 \Rightarrow \quad (1.3)$$

$\rho(t, f) \cdot \Delta t \cdot \Delta f =$ Fraction of the signal's energy at time Δt and frequency Δf

2. If we add all bits of energy from joint time-frequency density, we should get the total energy. That is;

$$\int_{-\infty}^{\infty} \int_{-\infty}^{\infty} \rho(t, f) dt \cdot df = \int_{-\infty}^{\infty} |x(t)|^2 dt = \int_{-\infty}^{\infty} |X(f)|^2 df = \text{Total energy of signal} \quad (1.4)$$

3. If we add up all bits of energy at a fixed frequency, we should get the energy density at that fixed frequency. Similarly, If we add up all bits of energy at a fixed time, we should get the energy density at that fixed time. These are called marginal densities.

That is;

$$\int_{-\infty}^{\infty} \rho(t, f) dt = |X(f)|^2 \quad \text{and} \quad \int_{-\infty}^{\infty} \rho(t, f) df = |x(t)|^2 \quad (1.5)$$

4. If the original signal is translated by a specific time t_0 , then the whole joint time-frequency density should be translated by that time. Similarly if the original signal is translated by a specific frequency f_0 , then the whole joint time-frequency density should be shifted by the same frequency f_0 . These are called time shift and frequency shift properties respectively. That is;

$$x(t) \Rightarrow x(t + t_0) \quad \text{then} \quad \rho(t, f) \Rightarrow \rho(t + t_0, f) \quad (1.6)$$

$$X(f) \Rightarrow X(f + f_0) \quad \text{then} \quad \rho(t, f) \Rightarrow \rho(t, f + f_0) \quad (1.7)$$

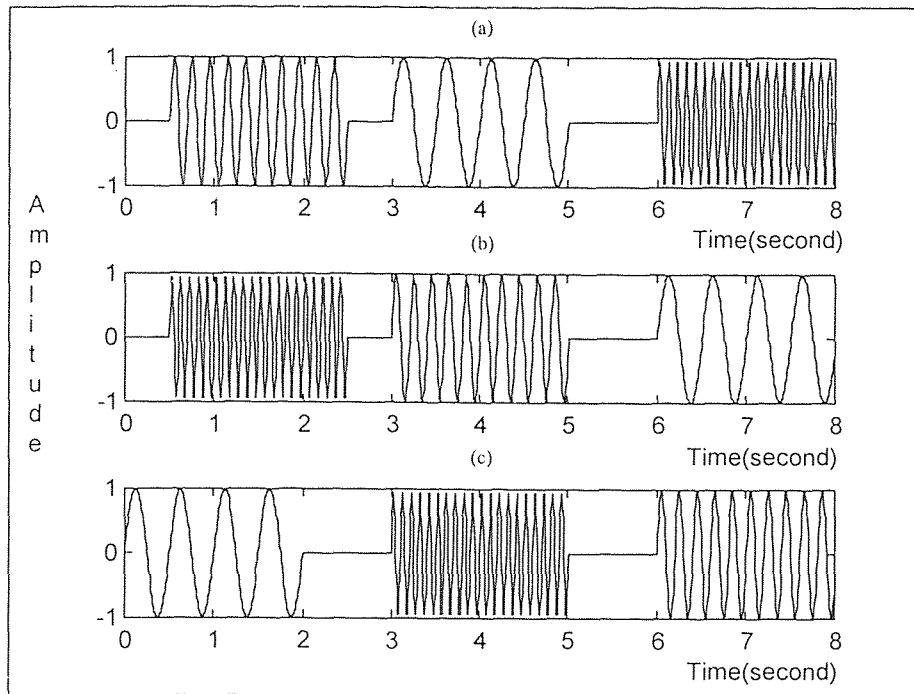


Figure 1 The plots of three finite duration signal. All signals contain same three frequencies (2, 5 and 10 hertz) except, it occurs at different time.

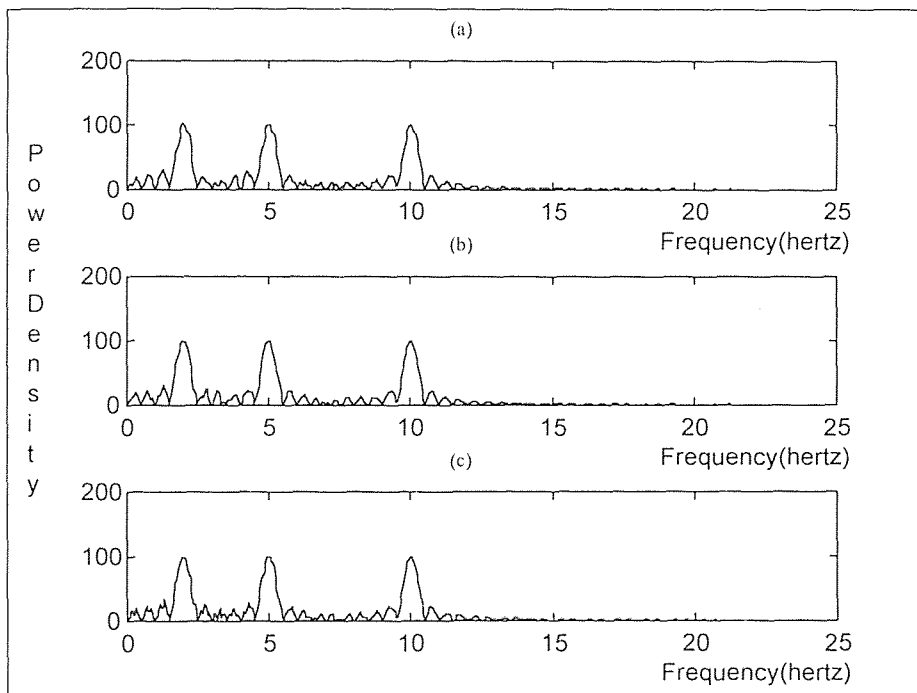


Figure 2 The plots of power spectrum for the three finite signal. The spectrum just tells us that frequencies existed at 2, 5 and 10 hertz.

5. For the joint time-frequency density function $\rho(t, f)$, its global average is given as;

$$\langle g(t, f) \rangle = \iint_{\infty} g(t, f) \cdot \rho(t, f) \cdot df \cdot dt \quad (1.8)$$

where $\langle g(t, f) \rangle$ is global average. The local or mean conditional value, the average of $g(t, f)$ at a particular time, is

$$\langle g(t, f) \rangle_t = \frac{\int_{\infty} g(t, f) \cdot \rho(t, f) \cdot df}{\int_{\infty} \rho(t, f) \cdot df} \quad (1.9)$$

and the local or mean conditional frequency (instantaneous frequency) should be;

$$\langle f \rangle_t = \frac{\int_{\infty} f \cdot \rho(t, f) \cdot df}{\int_{\infty} \rho(t, f) \cdot df} \quad (2.0)$$

6. For the joint time-frequency density function $\rho(t, f)$, the mean time at a given frequency should present group delay. That is;

$$\langle t \rangle_f = \frac{\int_{\infty} t \cdot \rho(t, f) \cdot dt}{\int_{\infty} \rho(t, f) \cdot dt} \quad (2.1)$$

1.4 Joint Time-Frequency Analysis Illustration

Time-frequency analysis was performed for the same three cases “a”, “b” and “c” of section 1.1. This is summarized as follows;

Figure 3.a shows that at intervals of [0 , 2], [3 , 5] and [6 , 8] seconds of the signal,

frequencies of 5, 2 and 10 hertz exist respectively. Figure 3.b shows that at intervals of

[0 , 2], [3 , 5] and [6 , 8] seconds of the signal, frequencies of 10, 5 and 2 hertz exist respectively and at last figure 3.c, shows that at intervals of [0 , 2], [3 , 5] and [6 , 8] seconds of the signal, frequencies of 2, 10 and 5 hertz exist respectively.

As we described in section 1.1 the draw back of time and frequency analysis was that it did not tell us when the different frequency components existed. However using time-frequency analysis one can fully describe the existence of a specific frequency at each instant of time. Source codes of the generated signals are presented in appendix A.

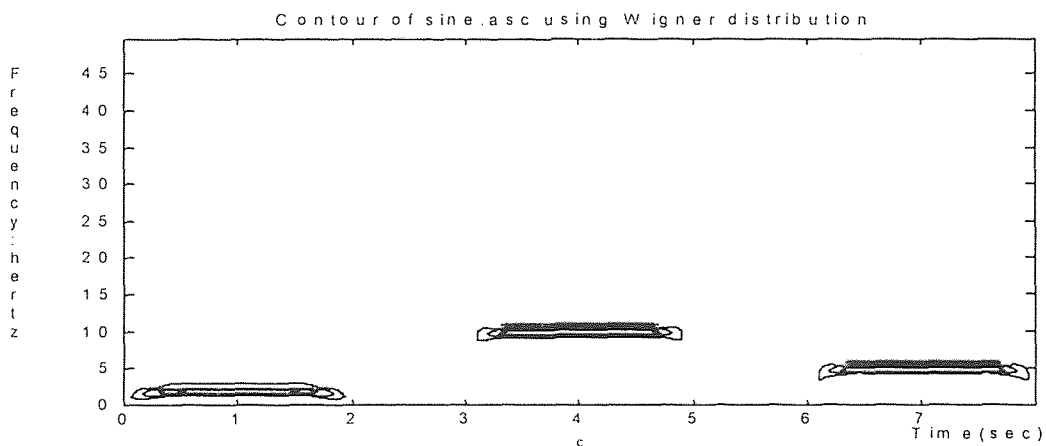
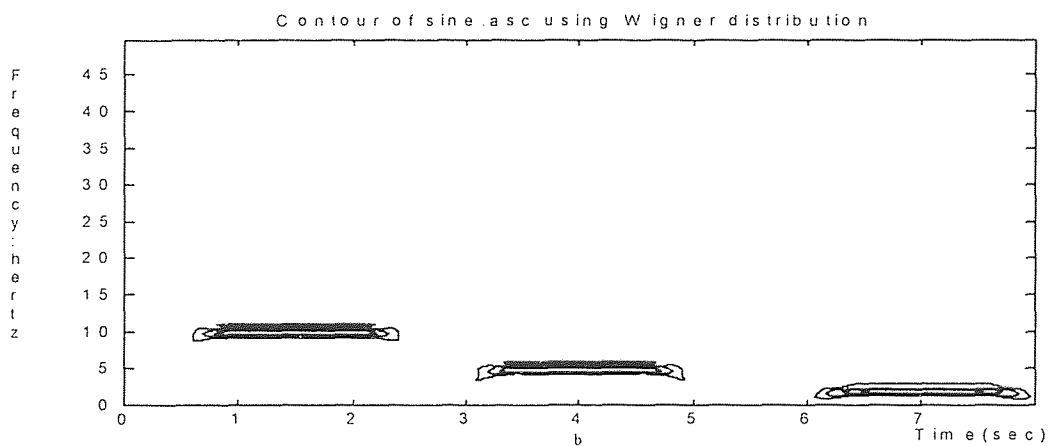
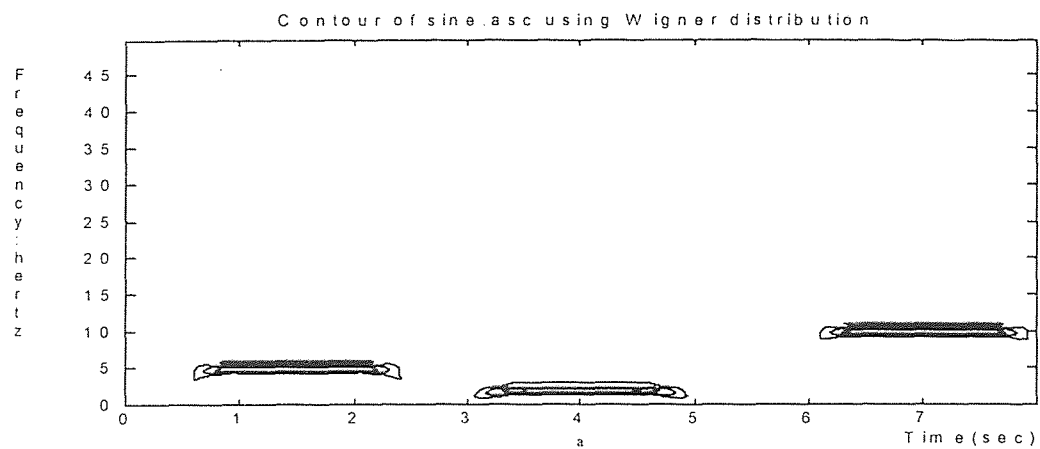


Figure 3 The contour plot of time frequency analysis of three finite duration signal

CHAPTER 2

CATEGORIZATION OF TIME-FREQUENCY DISTRIBUTIONS

2.1 Linear Time-Frequency Distribution

All linear time-frequency distributions (TFD) satisfy the superposition or linearity principle which states that if $x(t)$ is a linear combination of some signal components, then the TFD of $x(t)$ is the same linear combination of the TFDs of each of the signal components[3].

$$x(t) = c_1 x_1(t) + c_2 x_2(t) \Rightarrow \rho_x(t, f) = c_1 \rho_{x_1}(t, f) + c_2 \rho_{x_2}(t, f) \quad (2.1)$$

where $\rho_x(t, f)$, $\rho_{x_1}(t, f)$, $\rho_{x_2}(t, f)$ are time-frequency distributions of $x(t)$, $x_1(t)$, $x_2(t)$ respectively and c_1 , c_2 are constant coefficients.

Linearity is a desirable property in any application involving multicomponent signals (each part of a signal has its own identity) because there exist powerful analysis techniques for signals with such a property. One linear TFD of basic importance is the short-time Fourier transform and the basic idea is that: we can extract a small piece of the signal and take its Fourier transform and by continuing this process we can show the existing frequency components at each instant of time.

2.2 Bilinear Time-Frequency Distribution

Although linearity of the TFD is a desirable property, the bilinear(quadratic) structure of

a TFD is an intuitively reasonable assumption when we want to translate a TFD as a time-frequency energy distribution, since energy is a quadratic signal representation. All quadratic TFD satisfies the quadratic superposition principle which is defined as[3]

$$x(t) = c_1 x_1(t) + c_2 x_2(t) \Rightarrow \quad (2.2)$$

$$\rho_x(t, f) = |c_1|^2 \rho_{x_1}(t, f) + |c_2|^2 \rho_{x_2}(t, f) + c_1 c_2 \rho_{x_1 x_2}(t, f) + c_2 c_1 \rho_{x_2 x_1}(t, f) \quad (2.3)$$

where $\rho_x(t, f)$, $\rho_{x_1}(t, f)$ and $\rho_{x_2}(t, f)$ are the auto-time-frequency distributions of $x(t)$, $x_1(t)$, $x_2(t)$ respectively and c_1 , c_2 are constant coefficients.

The description of terms $\rho_{x_1 x_2}(t, f)$ and $\rho_{x_2 x_1}(t, f)$ are presented as follows:

Defining an expression of the form[5,6]

$$B = \sum_{j=1}^n \sum_{k=1}^n a_{jk} x_j y_k \quad (2.4)$$

where the a_{jk} are numbers, is called a bilinear form in the $2n$ variables x_1, \dots, x_n and

y_1, \dots, y_n . Writing B at length, we have

$$\begin{aligned} B = & a_{11}x_1y_1 + a_{12}x_1y_2 + \dots + a_{1n}x_1y_n \\ & + a_{21}x_2y_1 + a_{22}x_2y_2 + \dots + a_{2n}x_2y_n \\ & \dots \dots \dots \dots \dots \dots \dots \dots \\ & + a_{n1}x_ny_1 + a_{n2}x_ny_2 + \dots + a_{nn}x_ny_n \end{aligned} \quad (2.5)$$

The n -rowed square matrix $A = (a_{jk})$ is called the coefficient matrix of the form.

Introducing the vectors

$$\mathbf{x} = \begin{bmatrix} x_1 \\ \cdot \\ \cdot \\ \cdot \\ x_n \end{bmatrix} \quad \text{and} \quad \mathbf{y} = \begin{bmatrix} y_1 \\ \cdot \\ \cdot \\ \cdot \\ y_n \end{bmatrix}$$

we may write

$$B = \mathbf{x}^T A \mathbf{y} \quad (2.6)$$

where $\mathbf{x}^T = [x_1 \quad \dots \quad x_n]$ is the transpose of \mathbf{x} . This follows immediately from the definition of matrix multiplication.

If $\mathbf{y} = \mathbf{x}$, then (2.4) is called a quadratic form in the n variables x_1, \dots, x_n . Denoting this form by Q , we have

$$Q = \sum_{j=1}^n \sum_{k=1}^n a_{jk} x_j x_k \quad \text{or} \quad Q = \mathbf{x}^T A \mathbf{x} \quad (2.7)$$

Since the signal $x(t)$ is made of two components $x_1(t)$ and $x_2(t)$, we evaluate equation (2.7) for $n = 2$ and carrying multiplication of matrixes.

$$Q = \mathbf{x}^T A \mathbf{x} = \begin{bmatrix} x_1 & x_2 \end{bmatrix} \begin{bmatrix} a_{11} & a_{12} \\ a_{21} & a_{22} \end{bmatrix} \begin{bmatrix} x_1 \\ x_2 \end{bmatrix} = \begin{bmatrix} x_1 & x_2 \end{bmatrix} \begin{bmatrix} a_{11}x_1 + a_{12}x_2 \\ a_{21}x_1 + a_{22}x_2 \end{bmatrix} \quad (2.8)$$

$$Q = a_{11}x_1^2 + a_{12}x_1x_2 + a_{21}x_2x_1 + a_{22}x_2^2 \quad (2.9)$$

Note that to each pair of x_1 and x_2 there corresponds a cross components x_1x_2 and x_2x_1 .

By analogy, we define $c_1c_2\rho_{x_1,x_2}(t, f)$ and $c_2c_1\rho_{x_2,x_1}(t, f)$ in equation 2.3 as the cross terms which are bilinear in the signals $x_1(t)$ and $x_2(t)$.

Writing Q using equation (2.7) at length and taking corresponding terms $a_{jk}x_jx_k$ and $a_{kj}x_kx_j$ together, we obtain:

$$\begin{aligned} Q = & a_{11}x_1^2 + (a_{12} + a_{21})x_1x_2 + \dots + (a_{1n} + a_{n1})x_1x_n \\ & + a_{22}x_2^2 + \dots + (a_{2n} + a_{n2})x_2x_n \\ & + \dots \\ & + a_{nn}x_n^2. \end{aligned} \quad (2.10)$$

Thus, for an n -component signal $x(t)$ the TFD $\rho_x(t, f)$ will comprise n signal terms and $\binom{n}{2} = n(n-1)/2$ cross terms[3], a fact that makes the visual analysis of the TFD of multicomponent signals difficult.

Among all the bilinear TFD, The Wigner distribution (WD) is the most widely studied and applied. The Wigner distribution (WD) is defined as:

$$\rho_w(t, f) = \int_{-\infty}^{\infty} z\left(t - \frac{\tau}{2}\right) \cdot z^*\left(t + \frac{\tau}{2}\right) \cdot e^{-j2\pi f\tau} d\tau \quad (2.11)$$

where $z(t)$, $z^*(t)$ are the signal and the complex conjugate of the signal respectively and $\rho_w(t, f)$ is the Wigner distribution (WD).

From equation (2.11) we see that for a particular time we are adding up pieces made from the product of the signal at a past time multiplied by the signal at a future time, where the time into the past is equal to the time into the future.

2.3 Analytic Signal

In practical cases, the signals to be analyzed are real. An analytic signal $z(t)$ is a complex-valued signal whose spectrum is single-sided ($Z(f) \neq 0$ for $f > 0$ or $f < 0$). Because of this property of its spectrum, the imaginary part of an analytic signal is the Hilbert transform of the real part.

The Hilbert transform is defined as[4]:

$$\tilde{x}(t) = \frac{1}{\pi} \int_{-\infty}^{\infty} \frac{x(\lambda)}{t - \lambda} d\lambda \quad (2.12)$$

where $\tilde{x}(t)$ is the Hilbert transform of the signal $x(t)$.

Thus, to generate an analytic signal from a given signal $S_{original}(t)$, one should take the Hilbert transform of $S_{original}(t)$ which would become the imaginary part of analytic signal.

$$S_{\text{Im}}(t) = \frac{1}{\pi} \int_0^{\infty} \frac{S_{original}(\lambda)}{t - \lambda} d\lambda \quad (2.13)$$

Note, the lower limit of the integral is zero, because $S_{original}(t)$ is a physical signal and is valid for the time interval $[0, \infty)$. Define $S_{\text{Re}}(t) = S_{original}(t)$,

Then;

$$z(t) = S_{\text{Re}}(t) + jS_{\text{Im}}(t) \quad (2.14)$$

where $z(t)$ is an analytic signal.

There are three basic reasons for using the analytic signal in calculating a joint time-frequency distribution[2]. One of the reasons will be presented in next chapter and the other two are discussed below:

First, the analytic signal does not have negative frequencies and therefore can not cause interference terms with positive frequencies, although it does not eliminate the interference of the positive frequencies with other positive frequencies. There will always be interference terms, no matter what part of the signal is eliminated, since that is an inherent property of bilinear distributions.

Second, consider a real signal $s(t)$. Its energy density spectrum, $|S(f)|^2$ is always symmetric about the origin. This is illustrated in figure 4. Note, the average frequency

will always become zero which is not what we want because it does not give us a sense of what is really going on with the signal. Also we want to obtain a value for average frequency which is roughly centered in the middle of the right hand bump. To achieve that, we have to neglect the left bump in the averaging. This is illustrated as follows:

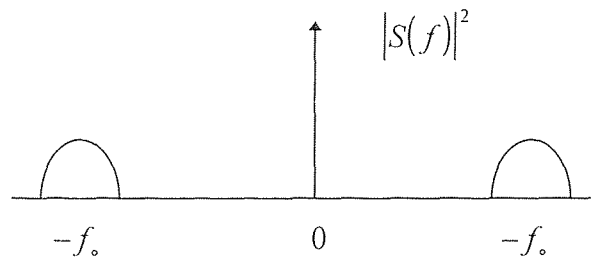


Figure 4 Energy density spectrum

Take the spectrum of the real signal $s(t)$

$$S(f) = \int_{-\infty}^{\infty} s(t) \cdot e^{-j2\pi ft} \cdot dt \quad (2.15)$$

Delete the negative part of the spectrum $S(f)$ such that;

$$S(f) \neq 0 \text{ for } f > 0 \text{ and } S(f) = 0 \text{ for } f < 0 \quad (2.16)$$

Take the inverse Fourier transform of the positive part of $S(f)$ to form the new complex signal $z(t)$. It turns out that the real part of signal $z(t)$ is the real signal $s(t)$ and the imaginary part is the Hilbert transform of $s(t)$ which is the definition of an analytic signal. Thus, to calculate the instantaneous frequency, the analytic signal should be used.

2.4 General Class of Time-Frequency Distributions

Most popular time-frequency representations can be expressed in terms of the general bilinear time-frequency distribution representations proposed by Dr. Leon Cohen. This allows one to generate all time-frequency distributions via a simple procedure. The mathematical formulation for the general class is [1];

$$\rho_z(t, f) = \iiint_{-\infty}^{\infty} e^{j2\pi v(u-t)} \cdot g(v, \tau) \cdot z\left(u + \frac{\tau}{2}\right) \cdot z^*\left(u - \frac{\tau}{2}\right) \cdot e^{-j2\pi f\tau} \cdot dv \cdot du \cdot d\tau \quad (2.17)$$

The $g(v, \tau)$ is an arbitrary function called the kernel and it determines the characteristics of the time-frequency distribution. Note that z is an analytic signal and z^* is the complex conjugate of z . If the integration with respect to v is performed, then equation 2.17 becomes:

$$\rho_z(t, f) = \iint_{-\infty}^{\infty} G(t, \tau) z\left(u + \frac{\tau}{2}\right) \cdot z^*\left(u - \frac{\tau}{2}\right) \cdot e^{-j2\pi f\tau} \cdot du \cdot d\tau \quad (2.18)$$

and the discrete time equivalent of equation 2.18 is:

$$\rho_z(n, k) = \sum_{m=-M}^M \sum_{p=-M}^M G(p, m) \cdot z(n + p + m) \cdot z^*(n + p - m) \cdot e^{-j4\pi mk/N} \quad (2.19)$$

The advantage to using equation 2.19 is that once the desirable kernel is chosen the distribution is fixed. The kernels which generate some of the common distributions are given in table 1.

2.5 Kernel Function

The kernel is particularly useful to study time-frequency distributions. They are easily generated, and the properties of the distribution can be observed by examining the kernel.

Also, when a new distribution is considered its properties can readily be ascertained by examining its kernel. The kernel $g(\nu, \tau)$ can depend on time, frequency and the signal; however, we will consider the kernels which do not depend on the signal. The kernel $g(\nu, \tau)$ is a function of ν and τ only, where ν, τ are time index and lag index respectively.

2.5.1 Properties

Nonnegativity:

A distribution should be positive for all values of time and frequency because it indicates how much of the total energy is in a particular time-frequency cell. The question that arises here is: What is the significance of the negative and positive regions? It seems the positive part does very often contain a time-frequency structure consistent with what we expect. No one understands the meaning of the negative regions. Sometimes the nonnegativity and cross terms are closely related, since the cross terms in the time-frequency domain are, in general, fluctuating and produce a plethora of negativity. Thus, in many cases, suppression of cross terms accompanies reduction of negative values in magnitude.

Realness:

The bilinear distributions are in general not positive definite, which implies, they are not strictly proper joint density functions. It has been argued that at least the kernel should be real [13]. That is for a given TFD $\rho_z(t, f)$;

Table 1. Some distributions and their kernels[1].

Name	Kernel: $g(\nu, \tau)$	Distribution: $\rho(t, f)$
Wigner	1	$\int e^{-2j\pi\nu f} s^*\left(t - \frac{\tau}{2}\right) s\left(t + \frac{\tau}{2}\right) d\tau$
Wigner (windowed)	$h(\tau)$	$\int e^{-2j\pi\nu f} h(\tau) s^*\left(t - \frac{\tau}{2}\right) s\left(t + \frac{\tau}{2}\right) d\tau$
Margenau- Hill	$\cos(\pi\nu\tau)$	Real $s(t)S^*(f)e^{-2j\pi\nu f}$
Kirkwood- Rihaczek	$e^{j\pi\nu\tau}$	$s(t)S^*(f)e^{-2j\pi\nu f}$
sinc	$\frac{\sin(2\pi a\nu\tau)}{2\pi a\nu\tau}$	$\frac{1}{2a} \int \frac{1}{\tau} e^{-j2\pi\nu f} \int_{-a\tau}^{+a\tau} s^*\left(u - \frac{\tau}{2}\right) s\left(u + \frac{\tau}{2}\right) dud\tau$
Page	$e^{j\pi\nu \tau }$	$\frac{\partial}{\partial t} \left \int_{-\infty}^{\infty} s(t') e^{-j2\pi\nu t'} dt' \right ^2$
Choi- Williams	$e^{-\nu^2\tau^2/\sigma}$	$\iint \sqrt{\frac{\pi\sigma}{\tau^2}} e^{-\pi^2\sigma(u-t)^2/\tau^2 - j2\pi\nu f}$ $s^*\left(u - \frac{\tau}{2}\right) s\left(u + \frac{\tau}{2}\right) dud\tau$
Spectrogram	$\int h^*\left(u - \frac{\tau}{2}\right) e^{-2j\pi\nu u}$ $h\left(u + \frac{\tau}{2}\right) du$	$\left \int e^{-j2\pi f t} s(\tau) h(\tau - t) d\tau \right ^2$
Zhao- Atlas- Marks	$g_1(\tau) \frac{\sin(2\pi\nu \tau /a)}{\pi\nu}$	$\int g_1(\tau) e^{-j2\pi\nu f} \int_{- \tau /a}^{+ \tau /a}$ $s^*\left(u - \frac{\tau}{2}\right) s\left(u + \frac{\tau}{2}\right) dud\tau$

$$\rho_z(t, f) = \iiint_{\infty} e^{j2\pi v(u-t)} \cdot g(v, \tau) \cdot z\left(u + \frac{\tau}{2}\right) \cdot z^*\left(u - \frac{\tau}{2}\right) \cdot e^{-j2\pi f t} \cdot dv \cdot du \cdot d\tau \quad (2.20)$$

Take the complex conjugate;

$$\rho_z^*(t, f) = \iiint_{\infty} e^{-j2\pi v(u-t)} \cdot g^*(v, \tau) \cdot z^*\left(u + \frac{\tau}{2}\right) \cdot z\left(u - \frac{\tau}{2}\right) \cdot e^{j2\pi f t} \cdot dv \cdot du \cdot d\tau \quad (2.21)$$

$$\text{Let} \quad v \rightarrow -v \quad \text{and} \quad \tau \rightarrow -\tau \quad (2.22)$$

We have;

$$\rho_z^*(t, f) = \iiint_{\infty} e^{j2\pi v(u-t)} \cdot g^*(-v, -\tau) \cdot z^*\left(u - \frac{\tau}{2}\right) \cdot z\left(u + \frac{\tau}{2}\right) \cdot e^{-j2\pi f t} \cdot dv \cdot du \cdot d\tau \quad (2.23)$$

Therefore to assure that;

$$\rho_z(t, f) = \rho_z^*(t, f) \quad (2.24)$$

the kernel should satisfy;

$$g(v, \tau) = g^*(-v, -\tau) \quad (2.25)$$

Time and Frequency Shifts:

A desirable property is that if we translate the signal by amount t_0 , we expect the whole distribution to be translated by the same amount. Similarly, if we shift the spectrum by a fixed frequency f_0 , then the distribution should be shifted by the same amount. That is if $z(t)$, $s(t)$, $\rho_z(t, f)$ and $\rho_s(t, f)$ are signal, shifted signal, distribution of signal and distribution of shifted signal respectively then;

$$s(t) = z(t - t_0) \Rightarrow \rho_s(t, f) = \rho_z(t - t_0, f) \quad (2.26)$$

Similarly;

$$s(t) = z(t) \cdot e^{j2\pi f_0 t} \Rightarrow \rho_s(t, f) = \rho_z(t, f - f_0) \quad (2.27)$$

The constraint for this property implies that the kernel should be independent of time and frequency.

Time and Frequency Marginals:

Another desirable property is that for a given time if we added up the bits of energy at different frequencies we will get the total energy $|z(t)|^2$ at that instant of time. Also if for a given frequency we add all the time pieces we should get the density in frequency. That is if $z(t)$, $\rho_z(t, f)$ are signal and distribution of signal respectively then;

$$\int \rho_z(t, f) df = z(t) \cdot z^*(t) = |z(t)|^2 \quad (2.28)$$

Similarly;

$$\int \rho_z(t, f) dt = Z(f)Z^*(f) = |Z(f)|^2 \quad (2.29)$$

Let us integrate the left hand side of equation 2.28

$$\int_{-\infty}^{\infty} \rho_z(t, f) \cdot df = \iiint_{-\infty}^{\infty} e^{j2\pi v(u-t)} \cdot g(v, \tau) \cdot z\left(u + \frac{\tau}{2}\right) \cdot z^*\left(u - \frac{\tau}{2}\right) \cdot e^{-j2\pi f\tau} \cdot dv \cdot du \cdot d\tau \cdot df \quad (2.30)$$

Using the definition of the Fourier transform we can write;

$$\int_{-\infty}^{\infty} e^{-j2\pi f\tau} \cdot df = \delta(\tau) \quad (2.31)$$

Hence

$$\int_{-\infty}^{\infty} \rho_z(t, f) \cdot df = \iiint_{-\infty}^{\infty} \delta(\tau) e^{j2\pi v(u-t)} \cdot g(v, \tau) \cdot z\left(u + \frac{\tau}{2}\right) \cdot z^*\left(u - \frac{\tau}{2}\right) \cdot dv \cdot du \cdot d\tau \quad (2.32)$$

$$\int_{-\infty}^{\infty} \rho_z(t, f) \cdot df = \iint_{-\infty}^{\infty} e^{j2\pi v(u-t)} \cdot g(v, 0) \cdot |z(u)|^2 \cdot dv \cdot du \quad (2.33)$$

The only way equation 2.33 can be made equal to $|z(t)|^2$ is to take

$$\int_{-\infty}^{\infty} e^{j2\pi v(u-t)} g(v,0) \cdot dv = \delta(t-u) \quad (2.34)$$

which forces;

$$g(v,0) = 1 \quad (2.35)$$

Similarly, we can show the condition on the kernel to satisfy the frequency marginal is

$$g(0,\tau) = 1 \quad (2.36)$$

Instantaneous Frequency:

If we fix time and ask for the expected value of frequency for that time, we obtain the first mean conditional frequency, given by:

$$\langle f \rangle_t = \frac{1}{\rho(t)} \int_{-\infty}^{\infty} f \cdot \rho(t,f) df \quad (2.37)$$

where $\rho(t)$ is the marginal in time

$$\rho(t) = \int_{-\infty}^{\infty} \rho(t,f) df \quad (2.38)$$

If the signal is analytic, the first moment of frequency for a given time is the instantaneous frequency because instantaneous frequency is defined in terms of the analytic signal. The instantaneous frequency is given in terms of the TFD:

$$\frac{\int f \cdot \rho_z(t,f) df}{\int \rho_z(t,f) df} = f_i(t) \quad (2.39)$$

where $f_i(t)$ is the instantaneous frequency. Constraint for the kernel is:

$$g(v,0) = 1 \quad \text{and} \quad \left. \frac{\partial g(v,\tau)}{\partial \tau} \right|_{\tau=0} = 0 \quad (2.40)$$

Group Delay:

From the point of view of joint time-frequency distributions we may think of the group delay as the mean time at a given frequency. Therefore everything we said for the expectation value of frequency at a given time allows us to write down the corresponding results for the expected value of time at a given frequency. That is

$$\frac{\int t \cdot \rho_z(t, f) dt}{\int \rho_z(t, f) dt} = \tau_g(f) \quad (2.41)$$

and the constraint for the kernel should be:

$$g(0, \tau) = 1 \quad \text{and} \quad \left. \frac{\partial \cdot g(v, \tau)}{\partial v} \right|_{v=0} = 0 \quad (2.42)$$

Time and Frequency Support:

For a finite duration signal the distribution should be zero before the signal starts and zero after the signal ends (weak finite support). But it would be much better if the distribution was zero whenever the signal was zero (strong finite support)[1]. We can apply the same concept to the frequency axis. That is, if the signal has a spectrum that ranges between two frequencies f_1 and f_2 and is zero otherwise, than the distribution should be zero for frequencies smaller than f_1 and for frequencies greater than f_2 . This is summarized as follows; For the time axis:

$$z(t) = 0 \quad \text{for} \quad |t| > t_c \Rightarrow \rho_z(t, f) = 0 \quad \text{for} \quad |t| > t_c \quad (2.43)$$

and on the frequency axis

$$Z(f) = 0 \quad \text{for} \quad |f| > f_c \Rightarrow \rho_z(t, f) = 0 \quad \text{for} \quad |f| > f_c \quad (2.44)$$

and the associated kernel requirements should be respectively:

$$\psi(t, \tau) \equiv \int g(v, \tau) e^{-j2\pi v \tau} dv = 0 \quad \text{for } |\tau| < 2|t| \quad (2.45)$$

$$\int g(v, \tau) e^{-j2\pi f \tau} d\tau = 0 \quad \text{for } |v| < 2|f| \quad (2.46)$$

Reduced Interference:

The distribution should not contain cross terms between frequency components. For a multicomponent signal, the spectrum of each signal should be clearly seen without interference. The constraint for the kernel is that $g(v, \tau)$ be a 2-D low pass filter type. The summary of above properties and associated kernel requirements are presented in table 2.

2.6 Ambiguity Function Relationship

Let $R_z(t, \tau)$ be the instantaneous autocorrelation of the a complex signal $z(t)$, defined as:

$$R_z(t, \tau) = z\left(t + \frac{\tau}{2}\right) z^*\left(t - \frac{\tau}{2}\right) \quad (2.47)$$

Then the symmetrical ambiguity function (AF) is defined as the inverse Fourier transform of $R_z(t, \tau)$ with respect to t.

$$A_z(v, \tau) = F_t^{-1}\left[R_z(t, \tau)\right] \quad (2.48)$$

This relationship may be combined with equation 2.17 to show that $\rho_z(t, f)$ may be found by:

$$\rho_z(t, f) = \iint_{\infty} A_z(v, \tau) \cdot g(v, \tau) \cdot e^{-j2\pi(v+f\tau)} \cdot dv \cdot d\tau \quad (2.49)$$

Thus, any member of Cohen's class of distributions may be found by first multiplying the kernel, $g(v, \tau)$, by the symmetric ambiguity function and then carrying out the double

Table 2. Distribution properties and associated kernel requirements[1].

Properties	Mathematical Description	Kernel Requirements
P0. Nonnegativity	$\rho_z(t, f) \geq 0 \forall t, f$	$g(v, \tau)$ is the AF of some $w(t)$
P1. Realness	$\rho_z(t, f) \in R$	$g(v, \tau) = g^*(-v, -\tau)$
P2. Time Shift	$s(t) = z(t - t_0) \Rightarrow$ $\rho_z(t, f) = \rho_z(t - t_0, f)$	$g(v, \tau)$ does not depend on t
P3. Frequency Shift	$s(t) = z(t) \cdot e^{j2\pi f_0 t} \Rightarrow$ $\rho_s(t, f) = \rho_z(t, f - f_0)$	$g(v, \tau)$ does not depend on f
P4. Time Marginal	$\int \rho_z(t, f) df = z(t) \cdot z^*(t) = z(t) ^2$	$g(v, 0) = 1$
P5. Frequency Marginal	$\int \rho_z(t, f) dt = Z(f)Z^*(f) = Z(f) ^2$	$g(0, \tau) = 1$
P6. Instantaneous Frequency	$\frac{\int f \cdot \rho_z(t, f) df}{\int \rho_z(t, f) df} = f_i(t)$	$g(v, 0) = 1$ and $\left. \frac{\partial g(v, \tau)}{\partial \tau} \right _{\tau=0} = 0$
P7. Group delay	$\frac{\int t \cdot \rho_z(t, f) dt}{\int \rho_z(t, f) dt} = \tau_g(f)$	$g(0, \tau) = 1$ and $\left. \frac{\partial \cdot g(v, \tau)}{\partial v} \right _{v=0} = 0$
P8. Time Support	$z(t) = 0$ for $ t > t_c \Rightarrow$ $\rho_z(t, f) = 0$ for $ t > t_c$	$\int g(v, \tau) e^{-j2\pi v \tau} dv = 0$ for $ \tau < 2 t $
P9. Frequency Support	$Z(f) = 0$ for $ f > f_c \Rightarrow$ $\rho_z(t, f) = 0$ for $ f > f_c$	$\int g(v, \tau) e^{-j2\pi f \tau} d\tau = 0$ for $ v < 2 f $
P10. Reduced Interference	$\rho_{z_1 * z_2}(t, f) = \rho_{z_2 * z_1}(t, f) = 0$	$\rho_z(v, \tau)$ is a 2-D low pass filter type

Fourier transform[1]. The generalized ambiguity function, $g(v, \tau)A(v, \tau)$ is a key concept which helps one in clearly seeing the effect of the kernel in determining $\rho_z(t, f)$.

We illustrate this concept in figure 5 [1], where the ambiguity function of two sine wave

signals is given. The auto terms of the two signals are placed near the center of figure 5 and the cross-terms are placed in the upper right and lower left corner. Thus, to determine a desirable distribution, the kernel function should emphasize the auto terms near the center and de-emphasize the cross terms in the corners.

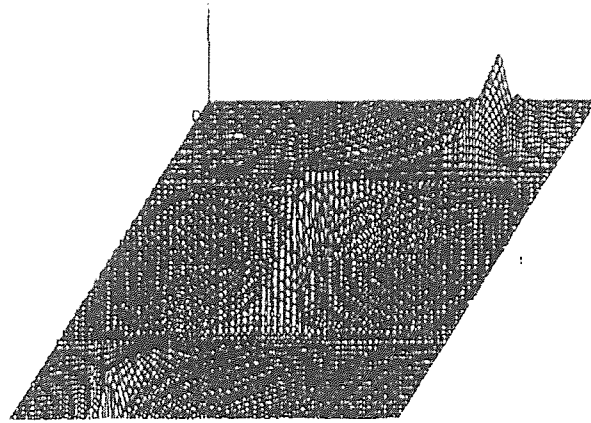


Figure 5 Ambiguity function of two sinewave signals

CHAPTER 3

COMPARISON OF TIME-FREQUENCY DISTRIBUTIONS

One of the facts regarding the time-frequency distribution is that so many plausible derivations and approaches have been suggested, yet the behavior of each distribution is dramatically different. In this chapter, I will present in depth some of the most popular time-frequency distribution with their properties, limitations, advantages and disadvantages.

3.1 Short Time Fourier Transform

The short time Fourier transform was the first tool devised for analyzing a signal in the time-frequency domain[13]. This is done by extracting a small piece of the signal and taking its Fourier transform and by continuing this process we show the existing frequency components at each instant of time. To present this idea mathematically we design a window function, $h(\tau - t)$ which will emphasize the times around the fixed time of interest t . We then multiply the signal with the window function and take its Fourier transform:

$$S_t(f) = \int_{-\Delta}^{+\Delta} s(\tau)h(\tau - t)e^{-j2\pi f\tau} d\tau \quad (3.1)$$

As we continue this process for each different time ,we get a different spectrum and the totality of these spectra makes a time-frequency distribution. The energy density of the

signal at the fixed time t is;

$$\rho_{sp}(t, f) = \left| \int_{-\Delta}^{t+\Delta} s(\tau)h(\tau - t)e^{-j2\pi f\tau} d\tau \right|^2 \quad (3.2)$$

where $\rho_{sp}(t, f)$ is called the spectrogram. The spectrogram can be also written in terms of the Fourier transforms of the signal and window function.

$$\rho_{sp}(t, f) = \left| \int_{f-\Delta}^{f+\Delta} S(f')H(f - f')e^{-j2\pi f' t} df' \right|^2 \quad (3.3)$$

where $H(f)$, $S(f)$ are Fourier transforms of the signal and window function respectively. Note, equation 3.3 can be used to study the behavior of the signal around the fixed frequency of interest f . The spectrogram should not be thought of as a different distribution because it is a member of a general class of distributions[2].

The questions that arise are, How large should the window be?, or , How should we weight each piece of the signal? To answer these questions we need to understand the uncertainty principle(time-bandwidth relation).

Let us define the duration of a signal $s(t)$ by Δt ;

$$(\Delta t)^2 = \int (t - \bar{t})^2 |s(t)|^2 dt \quad (3.4)$$

where \bar{t} is mean time and is defined as;

$$\bar{t} = \int t |s(t)|^2 dt \quad (3.5)$$

Let us also define the bandwidth of the signal $S(f)$ in the frequency domain by Δf ;

$$(\Delta f)^2 = \int (f - \bar{f})^2 |S(f)|^2 df \quad (3.6)$$

where \bar{f} is mean frequency and is defined as;

$$\bar{f} = \int f |S(f)|^2 df \quad (3.7)$$

The time bandwidth relation is;

$$\Delta t \cdot \Delta f \geq \frac{1}{4\pi} \quad (3.8)$$

The physical interpretation of time bandwidth is that the duration and bandwidth can not be both made narrow because $|s(t)|^2$ and $|S(f)|^2$ can not be changed independently[13].

The advantage of the short-time Fourier transform is that it has an easily understandable interpretation and is positive every where. This is a desirable property when we want to interpret the spectrogram as the signal energy distribution in the time-frequency plane.

One of the shortcomings of the short-time Fourier transform is the trade off between time and frequency resolution. If we choose a narrow(peaked) window $h(t)$ in the time domain then $H(f)$ becomes broad in the frequency domain. This results in high time resolution and poor frequency resolution. Conversely if we choose a window peaked in frequency, high frequency resolution is obtained but then $h(t)$ will be broad and poor time resolution is obtained. Consider two extreme choices of the analysis window $h(t)$. The first case is that of perfect time resolution, that is, if the analysis window $h(t)$ is a Dirac impulse,

$$h(t) = \delta(t) \Rightarrow \rho_{STFT}(t, f) = s(t)e^{-2j\pi ft} \quad (3.9)$$

where $s(t)$, $\rho_{STFT}(t, f)$ are the signal and short time Fourier transform of the signal respectively. In this case, the short time Fourier transform essentially reduces to the signal $s(t)$, preserving all time variations of the signal but not providing any frequency

resolution. The second case is that of perfect frequency resolution obtained with the all-constant window $h(t) = 1$, then;

$$H(f) = \delta(f) \Rightarrow \rho_{STFT}(t, f) = S(f) \quad (3.10)$$

where $H(f)$, $S(f)$ are Fourier transform of window and signal respectively. Here the short time Fourier transform reduces to the Fourier transform and does not provide any time resolution. Therefore, because of the uncertainty principle, both $h(t)$ and $H(f)$ can not be made arbitrarily narrow.

Another shortcoming of the spectrogram is that for a particular signal, a particular window may be more appropriate than another. Consider for example a signal which consists of two parts, one whose phase is sinusoidally modulated and another component whose frequency is increasing linearly.

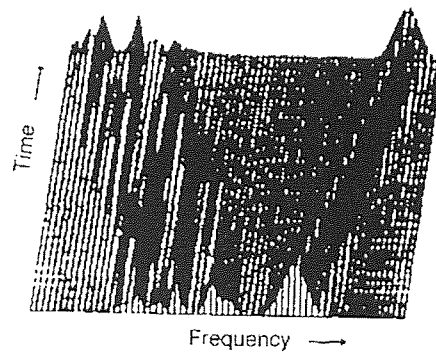


Figure 6 Spectrogram of a signal which consists of two components

The spectrogram of such a signal is illustrated in figure 6. Note we can not discern the sinusoidal modulation of the frequency of one of the components[1].

Also the spectrogram does not satisfy time and frequency marginal properties at the same instant. That is: if we write the signal $s(t)$ and window $h(t)$ in terms of their amplitudes and their phase;

$$s(t) = A(t)e^{j\theta(t)} \text{ and } h(t) = A_h(t)e^{j\theta_h(t)} \quad (3.11)$$

and similarly for their Fourier transforms

$$S(f) = B(f)e^{j\phi(f)} \text{ and } H(f) = B_h(f)e^{j\phi_h(f)} \quad (3.12)$$

Then the marginals are;

$$\int \rho_{STFT}(t, f) df = \int A^2(t') A_h^2(t' - t) dt' \quad (3.13)$$

$$\int \rho_{STFT}(t, f) dt = \int B^2(f') B_h^2(f - f') df' \quad (3.14)$$

These do not equal the instantaneous energy or energy density spectrum, namely

$A^2(t)$ and $B^2(f)$ [2]. But they do approach them as we narrow the window in the respective domains. However window $h(t)$ and $H(f)$ can not be narrowed simultaneously.

The short time Fourier transform is a linear signal decomposition and there are no cross terms between signal components. However, the spectrogram is a bilinear signal energy distribution due to the magnitude squaring operation. Thus, the spectrogram has cross terms but are not noticeable because they are inherently filtered out by a low-pass filter defined by the ambiguity function of the window [13].

3.2 Wigner Distribution

Among all the bilinear TFD, The Wigner distribution (WD) is the most studied and

applied [11]. The Wigner distribution can be obtained from the general

class (equation 2.17) by taking $g(\nu, \tau) = 1$:

$$\rho_w(t, f) = \int_{-\infty}^{\infty} z\left(t - \frac{\tau}{2}\right) z^*\left(t + \frac{\tau}{2}\right) e^{-2j\pi f\tau} d\tau \quad (3.11)$$

where $\rho_w(t, f)$, $z(t)$ and $z^*(t)$ are the Wigner distribution, an analytic signal and the complex conjugate of the analytic signal respectively. From equation (3.11) we see that for a particular time we are adding up pieces made from the product of the signal at a past time multiplied by the signal at a future time, where the time into the past is equal to the time into the future. The Wigner distribution satisfies many properties, which are described as follows:

The WD is a real valued function that is;

$$\rho_w(t, f) = \rho_w^*(t, f) \quad (3.12)$$

Since the kernel of the WD is one for any value of ν and τ , then the complex conjugate of the kernel is always one. That is;

$$g(\nu, \tau) = g^*(-\nu, -\tau) = 1 \quad (3.13)$$

This is the constraint of the kernel for the distribution to be real from section 2.5.1 .

The WD does satisfy the time and frequency shift properties as long as the kernel of the WD is not a function of time and frequency that is;

$$s(t) = z(t - t_0) \Rightarrow \rho_s(t, f) = \rho_z(t - t_0, f) \quad (3.14)$$

$$s(t) = z(t) \cdot e^{j2\pi f_0 t} \Rightarrow \rho_s(t, f) = \rho_z(t, f - f_0) \quad (3.15)$$

where $z(t)$, $s(t)$, $\rho_z(t, f)$ and $\rho_s(t, f)$ are the signal, the shifted signal, the distribution of

signal and the distribution of the shifted signal respectively. To prove this property one should take the kernel of the WD independent of time and frequency and set it equal to one, that is:

$$g(\nu, \tau) = 1 \text{ where } \nu \notin R_{time} \text{ and } \tau \notin R_{frequency} \quad (3.16)$$

Let $\rho_z(t, f)$, $\rho_s(t, f)$ represent the WD of the signal $z(t)$ and the shifted signal $s(t)$, then

$$\rho_s(t, f) = \int_{-\infty}^{\infty} z\left(t - \frac{\tau}{2} - t_0\right) z^*\left(t + \frac{\tau}{2} - t_0\right) e^{-2j\pi f \tau} d\tau \quad (3.17)$$

and

$$\rho_s(t, f) = \int_{-\infty}^{\infty} z\left(t - \frac{\tau}{2}\right) z^*\left(t + \frac{\tau}{2}\right) e^{-2j\pi f(\tau - t_0)} d\tau = \rho_z(t - t_0, f) \quad (3.18)$$

To prove the frequency shifting one can use a similar argument.

The WD is uniquely related to the signal up to a constant phase factor[2]. To understand this idea, take the inverse Fourier transform of equation 3.11 with respect to f ,

$$z\left(t - \frac{\tau}{2}\right) z^*\left(t + \frac{\tau}{2}\right) = \int \rho_w(t, f) e^{2j\pi f \tau} df \quad (3.19)$$

Then, let :

$$t + \frac{\tau}{2} \rightarrow t' ; t - \frac{\tau}{2} \rightarrow t \text{ and } \tau \rightarrow t - t'$$

which gives;

$$z(t) z^*(t') = \int \rho_w\left(\frac{1}{2}(t' + t), f\right) e^{2j\pi(t-t')f} df \quad (3.20)$$

Taking a particular value for $t' = 0$ and dividing both sides by $z^*(t')$, we obtain;

$$z(t) = \frac{1}{z^*(0)} \int \rho_w\left(\frac{1}{2}t, f\right) e^{j2\pi f t} df \quad (3.21)$$

One can therefore recover the original signal from the Wigner distribution for a given resolution. The preceding relation can be used to determine whether a signal exists which will generate a given $\rho_w(t, f)$.

The Wigner distribution also satisfies the marginals properties. To prove these, one can use the constraint of the kernel for marginals properties from section 2.5.1, that is;

$$g(v, 0) = 1 \text{ and } g(0, \tau) = 1 \quad (3.22)$$

By inspection, the kernel of the Wigner distribution $g(v, \tau) = 1$, satisfies both marginals. Since, the Wigner distribution satisfies both marginals properties, it will satisfy the total energy. Note the converse is not true[2]. For the first conditional moment at a fixed time, the Wigner distribution gives the instantaneous frequency and at a fixed frequency the first conditional moment would be the group delay.

For a finite duration signal the Wigner distribution is zero before the signal starts and after the signal ends[2]. To prove this, consider a finite duration signal in the interval t_1 to t_2 shown in figure 7:

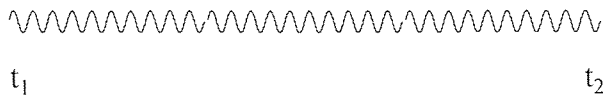


Figure 7 . Arbitrary finite signal

If we choose any point left of t_1 and fold over the signal to the right, there will be no

overlap since there is no signal to the left of t_1 to fold over. This will remain true, up to the start of the signal at time t_1 : Hence for finite duration signals, the Wigner distribution is zero up to the start. Similar arguments hold for points to the right of t_2 . Therefore for a time limited signal, the Wigner distribution is zero before the signal starts and after the signal ends. The same considerations apply to the frequency domain. If we have a band limited signal, the Wigner distribution will be zero for all frequencies that are not included in that band. These properties are called the support properties of the Wigner distribution. In general the Wigner distribution is not zero when the signal is zero[13]. To illustrate this idea consider the signal in figure 8:

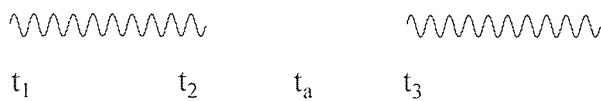


Figure 8 . Arbitrary finite signal

In the figure 8, the signal is zero from t_2 to t_3 . Focusing on point t_a and folding the right and left parts of t_a , it is clear that there will be an overlap. Hence the Wigner distribution is not zero even though the signal is. These overlaps causes difficulty in interpretation of the Wigner distribution.

Consider the multicomponent signal $z(t)$:

$$z(t) = z_1(t) + z_2(t) \quad (3.23)$$

The Wigner distribution is:

$$\rho_w(t, f) = \rho_{w_{11}}(t, f) + \rho_{w_{22}}(t, f) + \rho_{w_{12}}(t, f) + \rho_{w_{21}}(t, f) \quad (3.24)$$

where $\rho_w(t, f)$, $\rho_{w_{11}}(t, f)$ and $\rho_{w_{22}}(t, f)$ are the auto Wigner distributions of $z(t)$, $z_1(t)$ and $z_2(t)$ respectively. The terms $\rho_{w_{12}}(t, f)$ and $\rho_{w_{21}}(t, f)$ are called the cross Wigner distributions. Therefore the Wigner distribution of the sum of the two signals is not the sum of their respective Wigner distributions. In general the Wigner distribution puts cross terms in between any two frequencies and any two times[2].

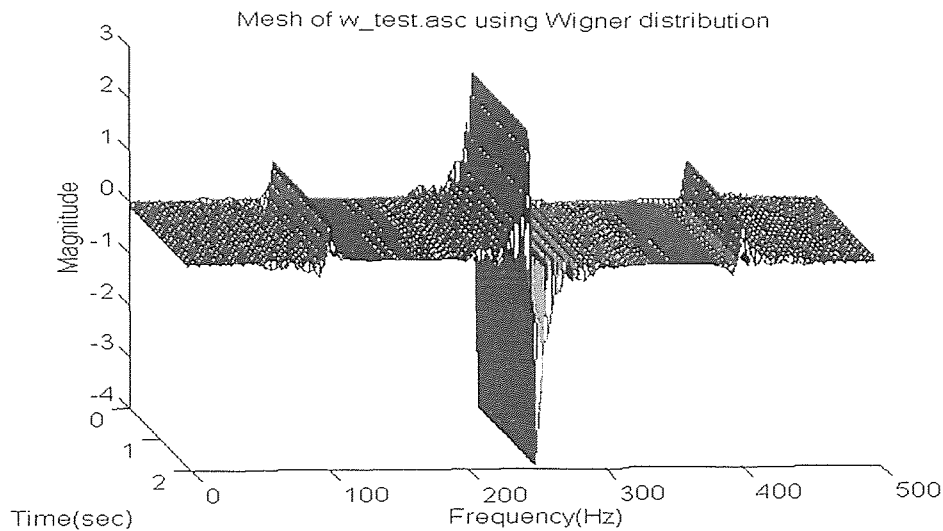


Figure 9 . The Wigner distribution of the sum of two finite duration sine waves. The oscillating term in the middle of the two frequencies is the cross term.

Figure 9 presents the Wigner distribution of a signal which is the sum of two sine waves of one second duration with frequencies of 100 and 400 hertz. Note the cross term in the middle of the two frequencies at 250 hertz. This is the most important draw back of the Wigner distribution (WD).

Another draw back of the Wigner distribution is that it always has negative regions throughout the time-frequency plane, except in the case of the Gaussian signal where the amplitude is modulated[1].

3.2.1 Windowed Wigner Distribution

In practice one is forced to calculate the Wigner distribution using equation 3.25:

$$\rho_w = \int_{t-\Delta}^{t+\Delta} h(\tau) z\left(t - \frac{\tau}{2}\right) z^*\left(t + \frac{\tau}{2}\right) e^{-2j\pi f\tau} d\tau \quad (3.25)$$

where $h(t)$ is a window function. This is due to the finite nature of the data. The resulting distribution has the effect of smoothing the Wigner distribution over frequency and is called the Pseudo Wigner distribution (PWD) [13]. The PWD sometimes results in a better looking distribution in that certain cross terms are suppressed. One can clean the cross terms by smoothing the Pseudo Wigner distribution over time which is called the Smoothed Pseudo Wigner distribution (SPWD). Smoothing the Pseudo Wigner distribution is performed as follows:

$$\rho_{ws}(t, f) = \iint_{\text{window}(L)} L(t - t', f - f') \cdot \rho_w(t', f') dt' df' \quad (3.26)$$

where L , $\rho_{ws}(t, f)$ and $\rho_w(t, f)$ are smoothing function, the Smoothed Pseudo Wigner distribution and the Pseudo Wigner distribution respectively. The advantages of the Smoothed Pseudo Wigner distribution are that for certain types of smoothing, a positive distribution is obtained and the cross terms are suppressed. However smoothing destroys some of the desirable properties of the Wigner distribution: if L is taken to be

independent of the signal, then the only way to obtain a positive distribution is by sacrificing the marginals properties[1].

3.3 The Exponential Distribution

A new approach has been presented by Choi and Williams where they address the main draw back of the Wigner distribution (cross terms)[13]. In section 3.2.1 a method was described to remove the cross terms but this usually involves violating some of the desired properties like the marginals. Choi and Williams investigated using a generalized ambiguity function [13]. They choose exponential kernel, that is;

$$g(v, \tau) = e^{-v^2 \tau^2 / \sigma} \quad (3.27)$$

Substituting equation 3.27 to in equation 2.17 and integrating with respect to v one obtains;

$$\rho_{cw}(t, f) = \iint \sqrt{\frac{\pi \sigma}{\tau^2}} e^{-\pi^2 \sigma (u-t)^2 / \tau^2 - j2\pi f} z^* \left(u - \frac{\tau}{2} \right) z \left(u + \frac{\tau}{2} \right) du d\tau \quad (3.28)$$

where $\rho_{cw}(t, f)$, $z(t)$ and $z^*(t)$ are the Choi-Williams distribution, an analytical signal and complex conjugate of the analytical signal. The ability to suppress the cross terms comes by controlling σ .

In figure 10, we illustrate three cases, where each contains two sine waves with frequencies of 100 and 400 hertz. The Choi Williams distribution was performed for the three cases but with different values for σ . Note, in case “a” we are taking σ to be 10000 which makes the kernel effectively one and we have the Wigner distribution. In case “b” and “c” we are taking σ to be 50 and 1, respectively which produces a kernel

which is peaked near the origin in the ν, τ plane and hence offers better cross term suppression.

Hence one can control the relative suppression of the cross terms by reducing the value of σ . The Choi Williams distribution satisfies many of the desirable properties, as described below:

The Choi Williams distribution is real. To prove this, one can replace the ν, τ with $-\nu, -\tau$ respectively in to the kernel function and perform the manipulation;

$$g^*(-\nu, -\tau) = e^{-(-\nu)^2(-\tau)^2/\sigma} = e^{-\nu^2\tau^2/\sigma} = g(\nu, \tau) \quad (3.29)$$

The Choi Williams distribution satisfies both the marginals properties, since;

$$g_{cw}(\nu, 0) = e^{-0^2\nu^2/\sigma} = 1 \quad (3.30)$$

and similarly for the other marginal. Since the marginal properties are satisfied, the total energy property will be satisfied.

The Choi Williams distribution does not satisfies the finite support properties. To show this we introduce the following condition for determining whether a distribution is zero before a signal starts and after the signal ends. This work was done by Claasen and Mecklenbrauker[11] and is expressed as follows:

$$\int g(\nu, \tau) e^{-j\nu t} d\nu = 0 \quad \text{for } |\tau| < 2|t| \quad (3.31)$$

Similarly, for the signal that is bandlimited in the region (f_1, f_2) the distribution should be zero for values of frequency less than f_1 and greater then f_2 .

$$\int g(\nu, \tau) e^{-j2\pi f t} d\tau = 0 \quad \text{for } |\nu| < 4\pi|f| \quad (3.32)$$

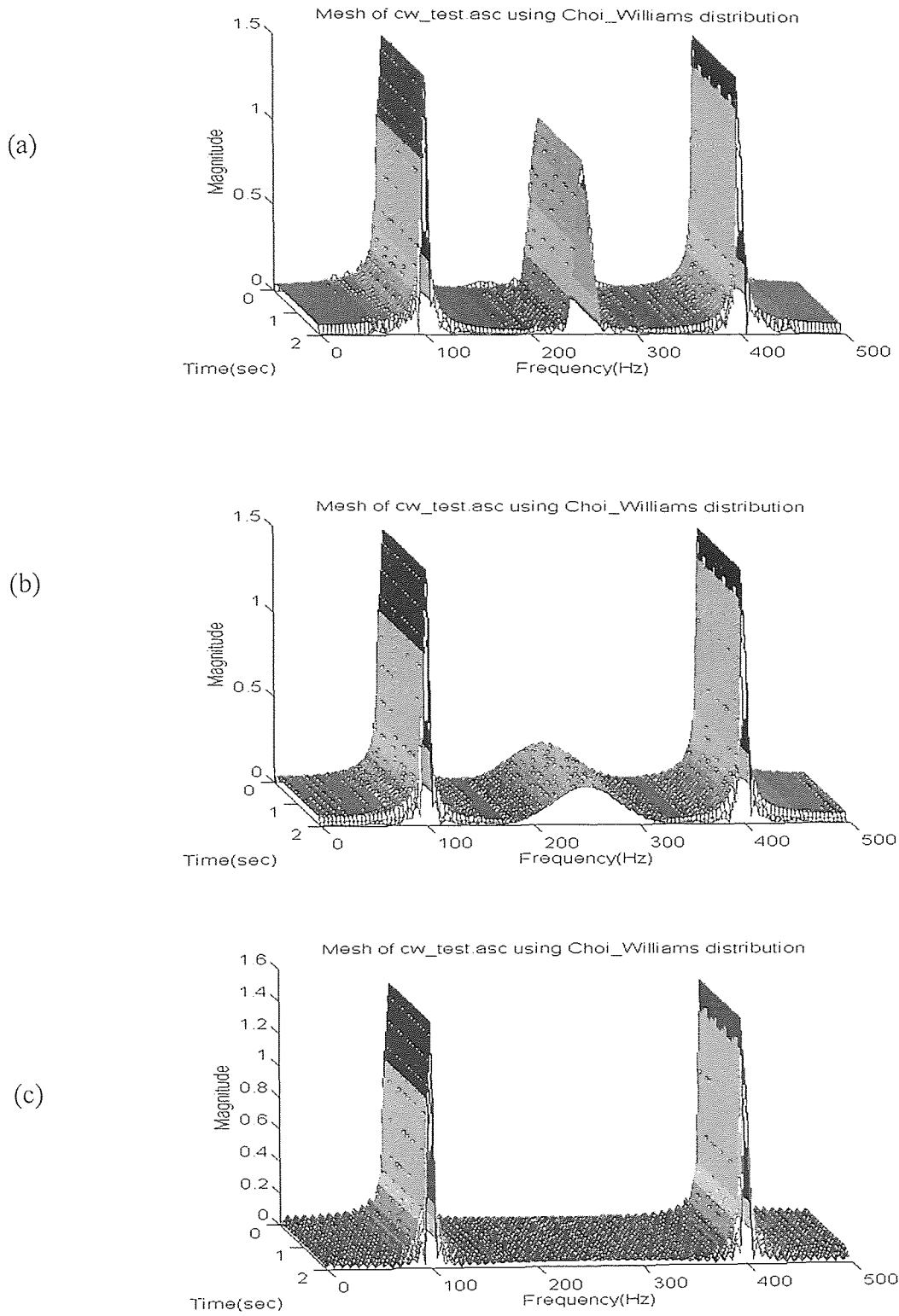


Figure 10 Performance of the Choi Williams distribution upon three cases with
 a) $\sigma = 1000$, b) $\sigma = 50$ and c) $\sigma = 1$.

If we replace the kernel of the Choi Williams distribution in equation 3.31 and carry out the integration using a table of integrals[11], we obtain:

$$\int e^{-v^2\tau^2/\sigma} e^{-2jv\tau} dv = \frac{\sqrt{\pi}}{\sqrt{\tau^2/\sigma}} e^{-\frac{t^2}{4\tau^2/\sigma}} \quad (3.33)$$

Note, the right hand side of equation 3.33 is not equal to zero, therefore The Choi Williams distribution does not satisfy the support properties.

3.4 Reduced Interference Distribution (RID)

Incorporating the idea of interference reduction in the Choi Williams distribution (P10 in Table 2) with other desirable properties (P0-P9 in Table 2), a new class of time-frequency distributions, called reduced interference distributions, has been introduced [9]. While not satisfying P0, the RID does satisfies P1-P10 and provides high resolution in time and frequency. To meet the requirements for P1-P10, the RID kernel should be a cross shaped low pass filter, satisfying [9]

$$|g(v,\tau)| \ll 1 \quad \text{for } |v\tau| > 0 \quad (3.34)$$

The following is the procedure to design a RID kernel[9].

Step 1: Design a primitive real valued function $h(t)$ that satisfies the following:

R1: $h(t)$ has unit area, i.e., $\int h(t)dt = 1$.

R2: $h(t)$ is a symmetrical function of time, i.e., $h(t) = h(-t)$.

R3: $h(t)$ is time limited on $[-1/2, 1/2]$, i.e., $h(t) = 0$ for $|t| > 1/2$.

R4: $h(t)$ tapers smoothly towards both ends so that its frequency response has little high

frequency content. That is, $|H(\nu)| \ll 1$ for $|\nu| \gg 0$, where $H(\nu)$ is the Fourier transform of $h(t)$.

Step 2: Take the Fourier transform of $h(t)$, i.e., $H(\nu) = \int h(t) e^{-j\nu t} dt$.

Step 3: Replace ν by $\nu\tau$ in $H(\nu)$: $g(\nu, \tau) = H(\nu\tau)$.

Since $g(\nu, \tau)$ is a function of the product of ν and τ , R1 implies that the RID satisfies both marginals properties. That is:

$$g(\nu, 0) = H(0) = \int h(t) e^{-j\nu t} dt = \int h(t) \cdot 1 dt = 1 \quad (3.35)$$

Similarly one can show the RID satisfies the frequency marginal. Condition R2 produces a real $H(\nu)$, which in turn implies the realness (P2) of the RID. Condition R2 also implies the instantaneous frequency and group delay exists under the condition that $\frac{dH(\nu)}{d\nu}$ exists[10]. The RID satisfies the time and frequency shift properties since the kernel does not depend on time or frequency. R3 does imply the time and frequency support properties[10]. To prove it, one should take the Fourier transform of the kernel with respect to ν and use the scaling property of the Fourier transform to carry out the integral. That is:

$$G(t, \tau) = \int g(\nu, \tau) e^{-j\nu t} d\nu = \frac{2\pi}{|\tau|} h\left(\frac{-t}{\tau}\right) \quad (3.36)$$

Based upon the kernel requirements in table 2, equation 3.36 has to equal zero in order to satisfy the time support. That is:

$$G(t, \tau) = \int g(\nu, \tau) e^{-j\nu t} d\nu = \frac{2\pi}{|\tau|} h\left(\frac{-t}{\tau}\right) = 0 \quad \text{if} \quad |\tau| < 2|t| \quad (3.37)$$

By symmetry, one can also show that the RID satisfies the frequency support. R4 plays the role of suppressing the interference. In most cases, the auto terms are located near the origin of the ambiguity domain, while the cross terms occur far away from the origin[9]. Therefore, a low pass filter type kernel imposed by R4 can effectively reduce interference's while retaining the resolution of the auto terms. Using a primitive function $h(t)$ designed according to requirements R1-R4, the RID has the following integral expression.

$$\rho_{RID}(t, f) = \iint \frac{1}{|\tau|} h\left(\frac{u-t}{\tau}\right) z\left(u + \frac{\tau}{2}\right) z^*\left(u - \frac{\tau}{2}\right) e^{-2j\pi f t} du d\tau \quad (3.38)$$

where $\rho_{RID}(t, f)$, $z(u)$ and $z^*(u)$ are the reduced interference distribution (RID), an analytical signal and complex conjugate of the analytical signal. The requirements on $h(t)$ and their counterparts are shown in table 3.

The RID is not dedicated to a certain type of signal. The idea underlying the RID is to develop TFDs that satisfy many desirable properties. One can find signals that will not be effectively handled by the RID; for example, a chirp. Since the RID has a cross shaped kernel in the ambiguity domain, if the ambiguity function of the chirp falls on a 45° diagonal line, then it will not intersect well with the RID kernel, resulting in low time and frequency resolution[9].

In this thesis we will present one example of a RID distribution where

$h(t) = \prod(t) = \prod_{-\frac{1}{2}}^{\frac{1}{2}} 1$. This corresponds to the Born Jordan distribution. It satisfies all of

R1-R4, and properties P1-P10 are satisfied. Since $h(t)$ is flat on $\left[-\frac{1}{2}, \frac{1}{2}\right]$, the resultant

$H(v\tau)$ has a very narrow bandwidth. Hence, the Born Jordan kernel provides very good

Table 3 Requirements on $h(t)$ and Their Counterparts

R1. unit area: $\int h(t)dt = 1$	P4 , P5
R2. symmetrical: $h(-t) = h(t)$	P1 , P6 , P7
R3. time limited: $h(t) = 0 \quad \forall t > \frac{1}{2}$	P8 , P9
R4. low pass type: $ H(v) \ll 0 \quad \text{for} \quad v \gg 0$	P10
Note: In this kernel design procedure, P2 and P3 are always satisfied, while P0 is not satisfied.	

interference at the expense of autoterm resolution[9]. The ambiguity domain kernel of the RID is shown in figure 11.

3.5 Implementation of Algorithm Using Matlab Software

This section presents algorithms which implement time-frequency signal analysis techniques on a computer system. Some of the Matlab code is presented. Matlab is a technical computing environment for high performance numeric computation and visualization. Matlab integrates numerical analysis, matrix computation, signal processing, and graphics in an easy to use environment. Matlab is an interactive system

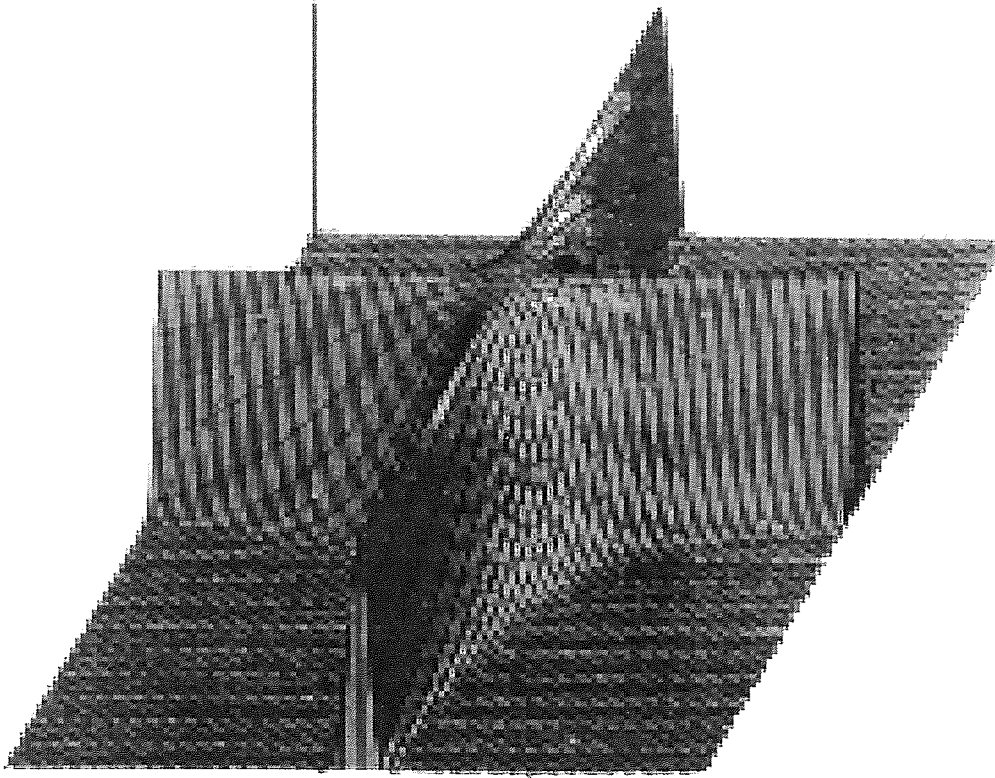


Figure 11 The ambiguity domain kernel of RID

whose basic data element is a matrix that does not require dimensioning. The most important feature of Matlab is its ease of extensibility.

Most time-frequency representations can be expressed in terms of the general bilinear time-frequency distribution. This is shown in equation 3.39

$$\rho_z(t, f) = \iiint_{-\infty}^{\infty} e^{j2\pi v(u-t)} \cdot g(v, \tau) \cdot z\left(u + \frac{\tau}{2}\right) \cdot z^*\left(u - \frac{\tau}{2}\right) \cdot e^{-j2\pi f\tau} \cdot dv \cdot du \cdot d\tau \quad (3.39)$$

where $z(t)$, $z^*(t)$ and $g(v, \tau)$ are an analytic signal, complex conjugate of the signal and the kernel function respectively. The expression used for discrete time implementation is the discrete time equivalent of equation 3.39, which is shown in equation 3.40 .

$$\rho_z(n, k) = \sum_{m=-M}^M \sum_{p=-M}^M G(p, m) \cdot z(n+p+m) \cdot z^*(n+p-m) \cdot e^{-j4\pi mk/N} \quad (3.40)$$

where $z(n)$ is an analytic signal.

3.5.1 Analytic Signal Calculation

In section 2.3 we pointed out the necessity of using an analytic signal in calculating a joint time-frequency distribution. The third reason for using an analytic signal is discussed below :

Equation 4.2 indicates that the discrete form of the general bilinear time-frequency distribution has a periodicity of $N/2$ rather than N . This is shown below:

$$e^{-j4\pi mk/N} = e^{\frac{-j2\pi mk}{N/2}}$$

Hence, even when the sampling of the signal satisfies the Nyquist criterion

$(f_{\text{sampling}} \geq 2f_{\text{max}})$, there are still aliasing components in the distribution. One way to ease this problem for practical purposes, is to increase the sampling frequency rate to twice the Nyquist rate. Another approach to avoid the aliasing is to use only the positive part of the signal's frequency components, the analytic signal. Using an analytic signal, N points of

a real signal are converted into $\frac{N}{2}$ points of its analytic signal. Therefore, aliasing is

eliminated and the sampling rate is reduced to the standard Nyquist rate. To generate an analytic signal for our purpose, we have used *hilbert.m* which is a built in function in Matlab[18]. This function will generate the analytic signal, that is: the real part of the result is the original real data, and the imaginary part is the actual Hilbert transform. The source code of *hilbert.m* is shown in appendix A.

3.6 General Approach to Computation of TFDs

The discrete time definition of Cohen's class of time-frequency distributions given in equation 4.2 forms the basis of the general approach to implementation of time-frequency distributions. This approach can be expanded to three steps[1]:

1. Form the bilinear product $K_z(n, m) = z(n+m)z^*(n-m)$. The bilinear product has Hermitian symmetry[6], that is:

$$K_z(n, m) = \begin{cases} z(n+m)z^*(n-m) & \text{for } m \geq 0 \\ K_z^*(n, -m) & \text{for } m < 0 \end{cases} \quad (3.41)$$

The following numerical example presents the idea of having Hermitian symmetry[5,6].

Given the complex matrix \mathbf{A} and calculating the conjugate transpose $\overline{\mathbf{A}}^T$ then $\overline{\mathbf{A}}^T = \mathbf{A}$;

$$\mathbf{A} = \begin{bmatrix} 4 & 1-3i \\ 1+3i & 7 \end{bmatrix}, \quad \text{then} \quad \overline{\mathbf{A}}^T = \begin{bmatrix} 4 & 1-3i \\ 1+3i & 7 \end{bmatrix}$$

This means that values of the bilinear kernel need only be calculated for positive time lags[6]. The efficient way to compute the bilinear product is to calculate them as they are required.

2. Convolve the bilinear product with the desired kernel function $G(n, m)$ in the n (time)

dimension for each time instant. In an actual implementation, either the product kernel matrix or the selection kernel matrix $G(n, m)$, may be computed at the point of use (in the convolution). This saves memory and time. Thus, the code was written in such way that the bilinear product will be computed at the point of use and selection kernel matrix $G(n, m)$ is calculated and stored. The kernel matrix $G(n, m)$ is known to be symmetrical in both time and lag dimensions, and so values are only used from the positive quadrant.

3. Calculate the discrete Fourier transform of this result, to produce the time slice of the desired distribution.

3.7 Code Fragments to Generate $G(n, m)$

This section shows example code fragments to generate the kernel matrix $G(n, m)$ [1].

Some TFDs and their determining kernel functions $G(n, m)$ are shown in table 4.

These code fragments were originally written in Fortran code. The equivalent codes for table 4, written for Matlab, are located in appendix A.

3.8 Optimization of Algorithm Using Matlab Software

Matlab works with essentially only one kind of object, a rectangular numerical matrix with the possibility of complex elements. In some situations, special matrices are allowed: 1-by-1 matrices, which are scalars, and matrices with only one row or one column, which are vectors[18]. Matlab also has control flow statements (for loops, while loops) like those found in most languages. The control flow statements of Matlab can be used as a complete high level matrix language. Disk files that contain Matlab statements(

ordinary ASCII text) are called *m-files* and are named with extension of “.m”. An *m-file* consists of a sequence of normal Matlab statements, including references to other *m-files* . An *m-file* can call itself recursively[18].

Table 4 TFDs and their determining function $G(n, m)$

Time-Frequency Representation	$G(n, m)$
Pseudo Wigner Distribution (PWD) using rectangular window	$\delta(n) \quad m \in \left[\frac{-(M-1)}{2}, \frac{(M-1)}{2} \right]$ 0 otherwise
Smoothed Pseudo Wigner Distribution using a rectangular window of odd length P	$\frac{1}{P} \quad n \in \left[\frac{-(P-1)}{2}, \frac{(P-1)}{2} \right]$ 0 otherwise
Rihaczek-Margenau	$\frac{1}{2} [\delta(n+m) + \delta(n-m)]$
STFT using a rectangular window of odd length P	$\frac{1}{P} \quad m+n \leq \frac{(P-1)}{2}$ 0 otherwise
Bon -Jordan- Cohn	$\frac{1}{ m +1} \quad m \leq n $ 0 otherwise
Choi-Williams (parameter σ)	$\frac{\sqrt{\sigma/\pi}}{2m} e^{-\sigma n^2/4m^2}$

Matlab's built-in vector and matrix operations are more than an order of magnitude faster than its compiler/interpreter operations[18]. This means that in order to obtain the most speed out of Matlab, every effort was made to vectorize the algorithms in our *m-files*.

Wherever possible, for and while loops have been converted to vector or matrix operations.

In places where we could not vectorize a piece of code, we preallocated any vectors in which output results were stored. If we did not preallocate, the Matlab interpreter has to resize the vector to one element larger each time through the iteration loop. Since the vector was preallocated, this step is eliminated and execution is faster. Also, since our program works with large matrices on computers with memory limitations, the preallocation uses memory much more efficiently in order to reduce fragmentation.

Thus, the code fragment that was presented in section 3.7 is not efficient in terms of execution time, speed and memory limitations. However, it can be used to trace the symmetries among the loops. Using the code symmetries, we wrote the program in the most vectorized form. Also, we preallocated most matrices before starting the calculations. The complete source code for the computation of time-frequency distributions is presented in appendix A.

Beside the implementation of the time-frequency distribution, we have also included other helpful algorithms, to:

- Detrend the input signal.
- Calculate the instantaneous frequency.
- Calculate the median frequency.

- To extract power spectral density for a certain range of frequency components.
1. By detrending the input signal, one can remove very low frequency components (near DC) from the signal. One should be very careful in detrending the signal because the frequency components very close to DC are lost in the detrending operation. For detrending, we have used the *filtfilt.m* function [18], which is zero-phase forward and reverse digital filtering. It operates in such a way that after filtering in the forward direction, the filtered sequence is reversed and run back through the filter. The resulting sequence has precisely zero-phase distortion and double the filter order.
 2. To calculate the instantaneous frequency, we used the fact that the first conditional moment of the distribution is instantaneous frequency.
 3. To calculate the median frequency, we used the fact that the median frequency is the frequency at which the area of the power density spectrum is divided into two equal portions[7].
 4. In order to study biological signal (vagal tone and sympatho-vagal balance), we developed an algorithm which calculates the area (power spectral density) under a designated band of frequencies for all time from the time-frequency distribution

matrix *TFDs*. Then, we used the ratio of these two area to calculate the sympatho-vagal balance[16]. The further description are presented in chapter 4.

The time-frequency distribution program is very user-friendly. It asks the user for certain input information and gives the option to do certain operations individually or as a group.

The results are presented in a 2-D or 3-D graph, which can be saved for further reference.

The typical questions asked by the time-distribution program are located in appendix A.

CHAPTER 4

APPLICATIONS OF TIME-FREQUENCY DISTRIBUTIONS

In this chapter, the basic concepts concerning the autonomic nervous system (ANS), structure and function of muscle and Data acquisition are briefly discussed. The PWD was applied to investigate the vagal tone and sympatho-balance during exercise on a bicycle. We then investigated the effect of detrending the signal using the SPWD. Other distribution such as, the Choi Williams and the Born Jordan distributions were applied toward the same signal. The SPWD was then applied to electromyographic signal (EMG) during muscle fatigue using different electrodes. We also compare our result from TFD with the spectral analysis of the EMG signal.

4.1 Autonomic Nervous System

One system that changes rapidly in the human body is the autonomic nervous system (ANS) [19]. The autonomic nervous system (ANS) is made up of two functional divisions: the sympathetic (SMP) division and the parasympathetic (PSMP) division. These two divisions are anatomically, physiologically and functionally distinct[20]. In general, the PSMP division enhances activities that gain and conserve energy, such as slowing down the heart. The SMP division increases energy expenditures and prepares an individual for action by accelerating the heart. When SMP and PSMP nerves innervate the same organ, they often (but not always) have antagonistic effects[20]. At rest there is

considerably more parasympathetic activity to the heart than sympathetic.

The interplay of the SMP and PSMP outflow plays an important role in the circulatory system. For the heart, sympathetic fibers terminate at the sinus node pacemaker, conduction system, atria, ventricles, and coronary vessels, while parasympathetic fibers in the vagus nerve terminate at the sinoatrial and atrioventricular nodes, atrial and ventricular musculature, and coronary vessels[21]. Although the inherent rhythmicity of the heart is due to a natural pacemaker situated in the sinoatrial node, continuous beat to beat control of the heart is dependent on the relative balance of the SMP and PSMP impulses delivered from the brain to the sinus node. From drug studies, three discrete frequency ranges in the spectrum of heart rate variability were found to be of importance: a very low frequency range(VLF, 0.02 to 0.06 Hz); a low frequency range (LF, 0.06 to 0.15 Hz); and a high frequency range (HF, 0.15 to 0.4 Hz) [22]. The VLF band was equated with the renin-angiotensin system; the LF band with blood pressure and baroreflex control, and the HF band with respiration. The HF band is mediated by parasympathetic pathways, while the LF band is mediated by both parasympathetic and sympathetic pathways.

Assessment of parasympathetic activity from spectral analysis is obtained via a measurement of the area under the HF peak. Sympathetic activity is less easy to quantify using this methodology [20]. A more realizable goal is that of the “sympatho vagal balance”, which recognizes both reciprocal and non-reciprocal parasympathetic and sympathetic influences on heart rate, with a further measure, the LF:HF ratio [20,25].

Factors other than the cardiac nerves can also alter heart rate (HR). The HR is also

sensitive to changes in body temperature, plasma electrolyte concentrations and hormones. However, those factors are normally of lesser importance than SMP and PSMP nerve pathways to the heart [24].

4.1.1 Protocol and Acquisition of InterBeat Interval

This protocol is designed using an exercise bicycle. The protocol consists of acquiring data two minutes prior to exercise (rest), six minutes of exercise at 70% of age predicted maximum heart rate and four minutes following the halt of the exercise (recovery). The IBI signal, which is derived from the patient's electrocardiogram, is stored in a single file to prevent the loss of any information during the run. The acquisition of the InterBeat interval (IBI) data was initially done by Fernando and collection can be found in his thesis [16].

4.1.2 Vagal Tone and Sympatho-vagal Balance via Time-Frequency Distribution during Exercise on a Bicycle.

This section looks at some applications of the time-frequency distribution techniques. As well, comparisons of different types of time-frequency distributions are done to find the best one for the sympatho-vagal balance case. First, we start with the problem of detrending a signal.

The Pseudo Wigner distribution(PWD) was calculated using our time-frequency distribution software. This distribution was then applied to the original (no detrending) IBI signal and detrended IBI signal. The details of the detrending process are described in chapter 3. The vagal tone was then obtained for the entire file by calculating the area

under the high frequency (HF) range for each instant of time. The sympatho-vagal balance (the ratio of the LF to HF range) was also obtained. As mentioned earlier drug studies indicate the LF range is a mixture of sympathetic and parasympathetic division activity. The ratio is an indication of both reciprocity and non-reciprocity [20].

The PWD was then applied to a detrended IBI signal from a normal healthy individual.

Figure 12 displays the typical response of a normal healthy individual to the protocol.

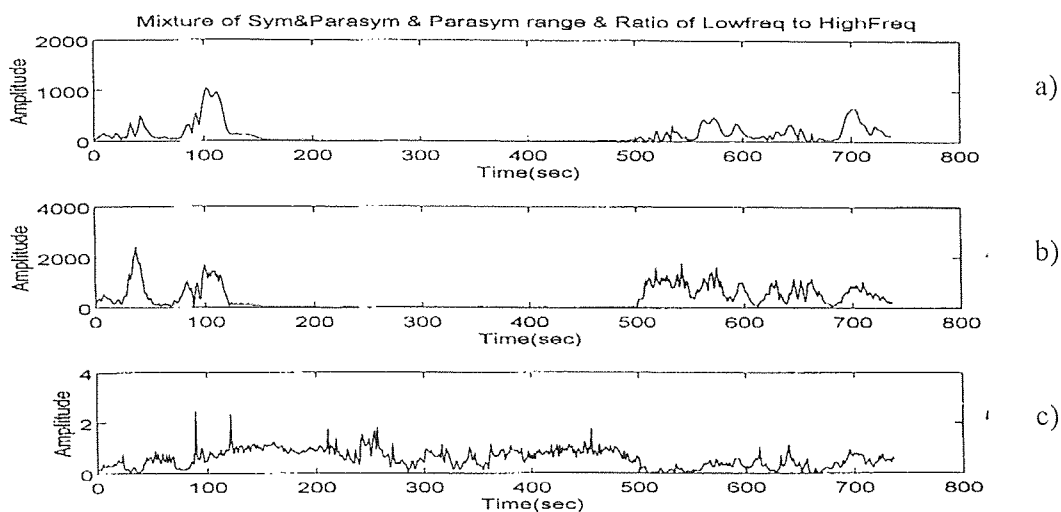


Figure 12 Applying PWD to IBI signal. a) sympathetic and parasympathetic b) vagal tone c) sympatho-vagal balance, during 2 minutes of rest(120 sec), 6 minutes of exercise (360 sec)and 4 minutes of recovery(240 sec) respectively

Figure 12.a displays a drop of vagal tone as the subject initiated exercise at the two minute mark. During the six minutes of exercise the vagal tone activity was suppressed. When the subject was asked to halt exercise at the 8 minute mark, the sympatho-vagal balance (figure 12.b) decreased to rest conditions. The PWD was then applied to the

original (non-detrended) IBI signal using the same subject. Figure 13 displays this response. Observing the graphs in figure 12 and 13, two facts are relevant. First, it is evident that the reciprocal relationship between the parasympathetic and sympathetic nervous systems influencing the heart is depicted. Second, figure 13 contains more information and it is more precise in the sense of the presentation of the frequency

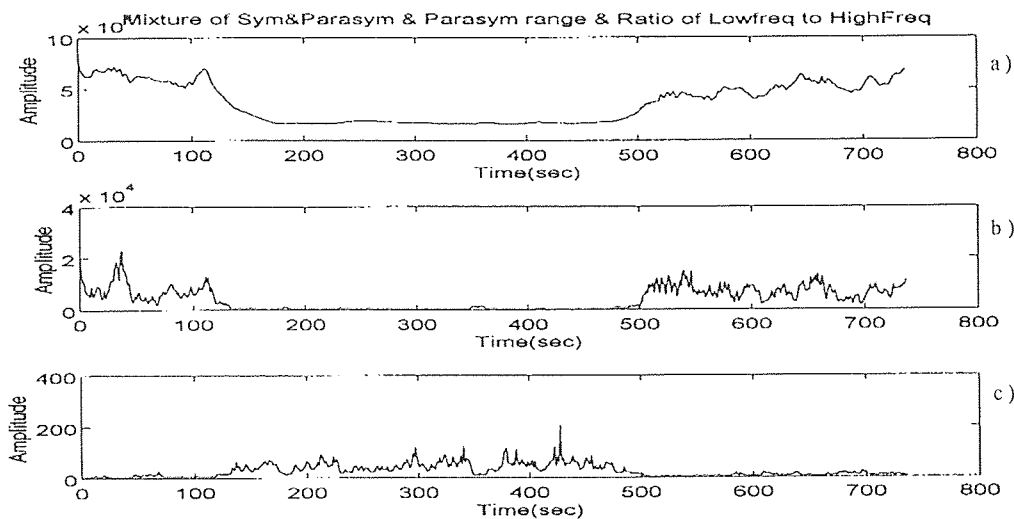


Figure 13 Applying PWD to IBI signal. a) sympathetic and parasympathetic b) vagal tone c) sympatho-vagal balance, during 2 minutes of rest(120 sec), 6 minutes of exercise (360 sec)and 4 minutes of recovery(240 sec) respectively

existing at a fixed time. That is due to the detrending process of the IBI signal. For detrending, we have used a low pass digital filter with cutoff frequency of 0.03 hertz. Since ideal filters cannot be implemented, and narrow band filters smear the frequency response, the IBI signal has lost some of its information due to the non-ideal filter. This loss occurs in the neighborhood of 0.03 hertz. We have analyzed all ten subjects that are presented in by Fernando's[16]. The behavior of the vagal tone and sympatho-vagal

balance are similar in all cases. Thus, in this technique extracting certain frequency bands does not require detrending the signal.

Taking advantage of our time-frequency distribution software, other distributions were then applied to the original (non-detrended) IBI signal using all ten subjects that are presented in by Fernando's[16]. Each distribution performed in the same way for all ten subjects. We used one of the subjects to present the behavior of each distribution. Since the PWD was already presented for one of the subject, we used the same one to demonstrate the responses of other distributions.

The SPWD was first applied to the original (non-detrended) IBI signal, results are shown in figure 14.

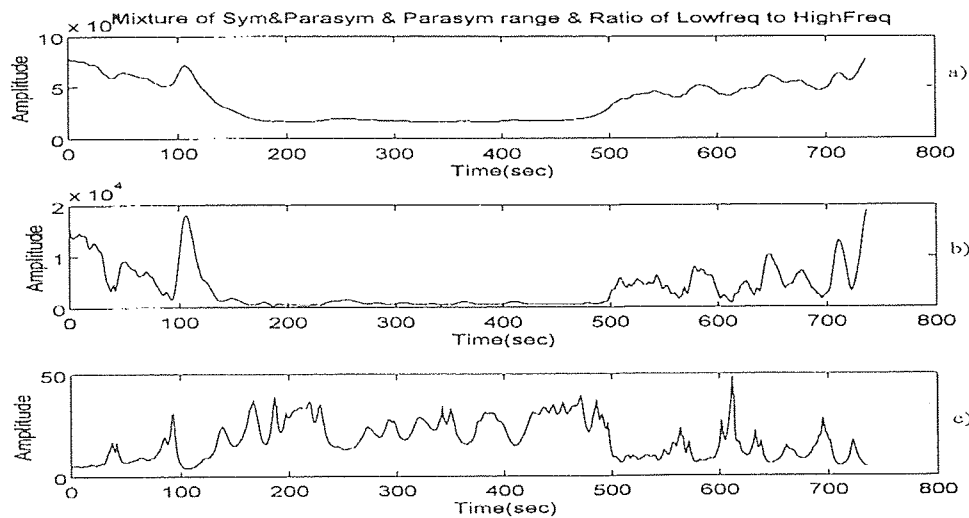


Figure 14 Applying SPWD to IBI signal. a) sympathetic and parasympathetic b) vagal tone c) sympatho-vagal balance, during 2 minutes of rest(120 sec), 6 minutes of exercise (360 sec)and 4 minutes of recovery(240 sec) respectively

Figure 14.b displays a drop of vagal tone as the subject initiated exercise at the two

minute mark. During the six minutes of exercise the vagal tone activity was suppressed. If the wave in figure 14.c were smoothed, the interval between two minutes and eight minutes will be higher in amplitude than the previous and following intervals.

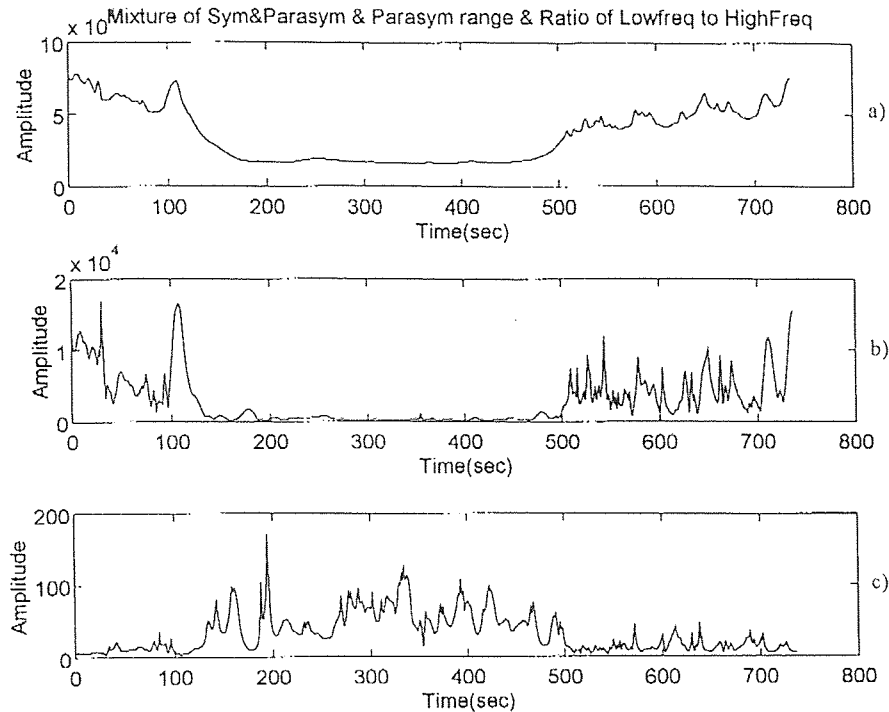


Figure 15 Applying CWD to IBI a) sympathetic and parasympathetic b) vagal tone c) sympatho-vagal balance, during 2 minutes of rest(120 sec), 6 minutes of exercise (360 sec) and 4 minutes of recovery(240 sec) respectively.

The Choi-Williams distribution(CWD) was then applied to the original (non-detrended) IBI signal. Figure 15.b displays clearly a drop of vagal tone as the subject initiated exercise at the two minute mark. During the six minutes of exercise the vagal tone activity was suppressed. When the subject was asked to halt exercise at the 8 minute mark, the sympatho-vagal balance(figure 15.c) decreased.

Next, the Born-Jordan distribution(BJD) was applied to the original (non-detrended) IBI signal. Figure 16 displays the response. At the two and eight minute marks, drop and rise of vagal tone (figure 16.b) was observed respectively. The sympatho-vagal balance (figure 16.c) looked different than the sympatho-vagal balance we obtained from other distributions. That is, the overall amplitude variation was very small (1 to 1.5) and the amplitude variation between the two and eight minute marks were much smaller than the overall amplitude variation.

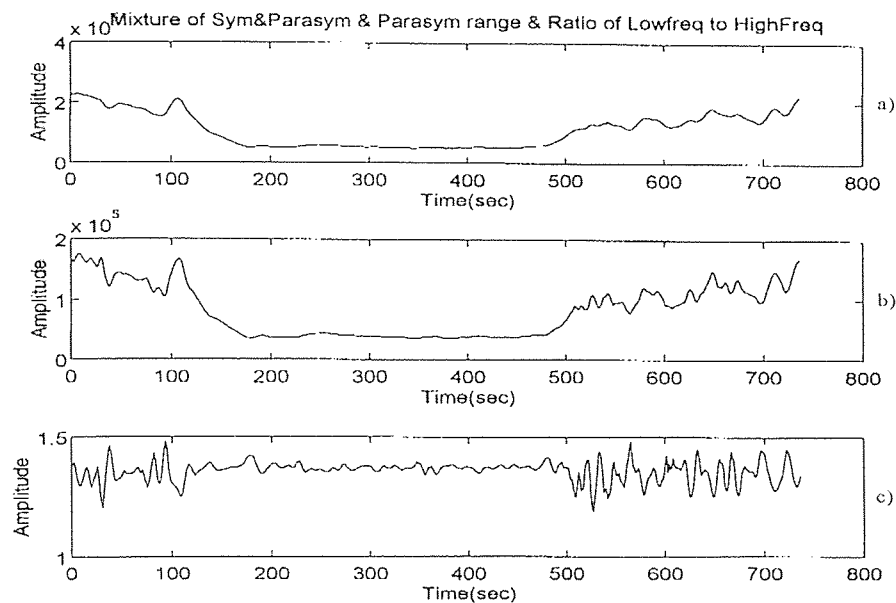


Figure 16 Applying BJD to IBI signal. a) sympathetic and parasympathetic b) vagal tone c) sympatho-vagal balance, during 2 minutes of rest(120 sec), 6 minutes of exercise (360 sec) and 4 minutes of recovery(240 sec) respectively.

In this case smoothing the interval between two minutes and eight minutes might show

that the amplitude is higher than the previous and following intervals.

Lastly, the Rihaczek-Margenau(RMD) distribution was applied to the original (non-detrended) IBI signal. Figure 17 displays the response. we can notice a drop of vagal tone (figure 17.b) as the subject initiated exercise at the two minute mark and suppression of vagal tone during the six minutes of exercise. Also when the subject was asked to halt exercise at the 8 minute mark, the sympatho-vagal balance (figure 17.c) decreased to rest conditions.

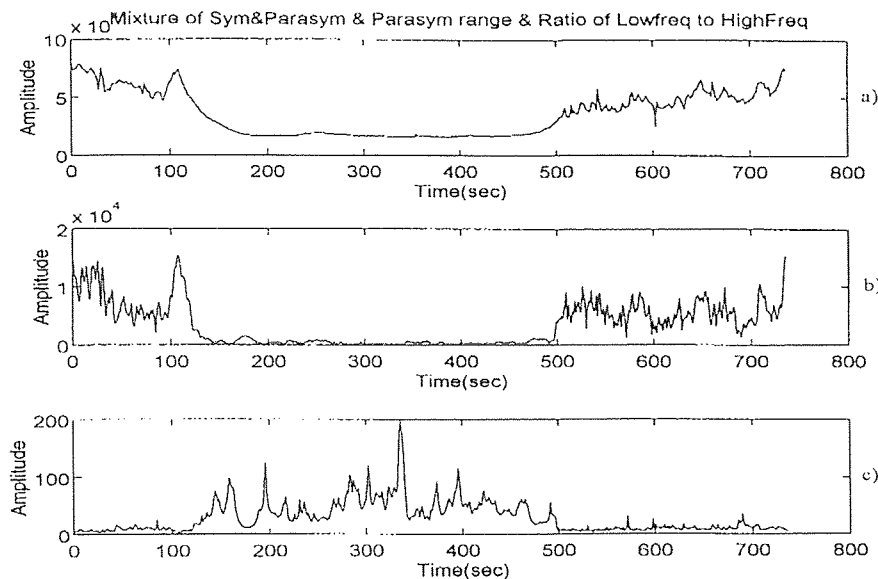


Figure 17 Applying RMD to IBI signal. a) sympathetic and parasympathetic b) vagal tone c) sympatho-vagal balance, during 2 minutes of rest(120 sec), 6 minutes of exercise (360 sec) and 4 minutes of recovery(240 sec) respectively.

We tried each distribution for all ten subject. For any of the subjects, we also used the same distribution with different parameters(length of analysis window, FFT length, skip point). Changing the size of analysis window, FFT length and skip points toward the

time-frequency calculation did not show any substantial changes. As can be seen in above demonstration, the responses of the different distribution showed similar kinds of activity and some different. There has been many arguments about using a particular distribution. One approach is to argue that the performance of a distribution is best for a particular property that is deemed desirable [2]. Another approach is that the choice of distribution should depend on the application and possibly the class of signals used [2]. For our future research, we decided to use the smoothed pseudo Wigner distribution (SPWD). The smoothed Wigner pseudo distribution contains many good properties of the Wigner distribution, but it also loses some of the properties. That is because of the selection of smoothing function. But some previous knowledge about the signal can help one to design a proper smoothing function for that particular signal. The smoothed pseudo Wigner distribution suppresses the cross terms, which is a desirable property when we are analyzing the biological signals. Also for certain types of smoothing, a positive distribution is obtained.

4.2 Physiology of Electromyographic Signal (EMG)

Skeletal muscle is composed of a large number of muscle fibers. Each muscle fiber is composed of many fibrils, and is filled with the contractile proteins, actin and myosin. These proteins are extremely well organized and are capable of slipping past each other when the calcium level in the muscle fiber increases [26]. As they slip past each other, the muscle fiber shortens and produces a force. The increased calcium level, which causes this contraction, is triggered by a muscle action potential that propagates along the

muscle. This muscle action potential is triggered by a nerve action potential that propagates down the motor nerve and innervates the muscle at the motor end plate. One motor nerve can innervate one or many muscle fibers. When an action potential reaches the motor end plate, the nerve releases a neurotransmitter (acetylcholine)[27]. Acetylcholine diffuses from the motor nerve to the muscle fiber and initiates a single muscle action potential (AP). The AP produces a single muscle twitch (contraction). Thus, a train of nerve action potentials will produce a train of muscle action potentials and a train of twitches. If the frequency of the nerve action potentials is high, the twitches summate and produce a contraction that is a function of the frequency of the action potentials. Further, other motor nerves will innervate other muscle fibers in the muscle, and recruiting additional motor nerves will produce greater muscle contractions and greater muscle forces[26]. Any muscle activation will produce many muscle action potentials that, while not totally synchronized, summate to produce an electromyogram.

4.2.1 Integrity of the EMG Signal

The characteristics of the EMG waveform depend on the type of electrode, the placement of the electrode, and the activity of the muscle. The bioelectric potentials associated with muscle activity can be measured at the surface of the body near the muscle of interest or directly from the muscle by penetrating the skin with needle or fine wire electrodes. In our experiment, we obtained an EMG signal using one pair of surface electrodes (surface active to surface reference) and three fine wire (Fw) electrodes (Fw#1 to Fw#2 and Fw#2 to Fw#3). The contractile fatiguability of muscles has been related to the muscle fiber

types that comprise a muscle. Muscles with predominantly slow twitch motor units (Type I) resistant to contractile fatigue more than those that are more evenly mixed with slow and fast twitch motor units or a predominance of fast (type II) fibers. In our research, the data is obtained from muscles with fast fibers (Type II).

A power spectrum of an electromyogram spans the frequency range of 10 - 3000 hertz with most of the power in the 50 to 60 hertz range[28]. An action potential of a muscle has a fixed magnitude, regardless of the intensity of the stimulus that generates the response. Increasing the firing rate of individual motor units or the number of motor units that fire will increase the muscle force.

4.2.2 Data Acquisition

The EMG signal from 3 different electrode configurations was fed to an isolated preamplifier (Gould #11-5407-58). This preamplifier in turn was connected to a signal conditioning universal amplifier (Gould #13-4615-58). In the amplifier, the signal was bandpass filtered between 10 Hz and 1000 Hz and amplified 200-600 times. The conditioned 3 analog data signals were fed into a 12 bit resolution analog to digital converter interface board (Keithley MetraByte #DAS1601) through screw terminal accessory kit (Keithly MetraByte #STA-16). The converted data were then stored in binary form in an IBM compatible 286 computer using data acquisition software (Keithley MetraByte # Streamer V3.5). The output of the signal conditioner units were monitored using a 4 channel digitizing oscilloscope (tektronix #TDS 455A) during muscle contraction to check for signal free of any noise or artifact. The details of data

collection is further explained in by Maniar [15].

4.2.3 Electromyographic Signal (EMG) via Time-Frequency Distribution during Muscle Fatigue

In the past, published studies have investigated the power density spectrum of the EMG signal to quantify metabolic muscle fatigue. The techniques limited application to muscles accessible by surface electrodes. Recent studies at the Kessler Institute for Rehabilitation have centered around the power spectral density technique. This type of analysis compares median frequency (MF) and decline in median frequency (MF) with fatigue using surface electrodes and fine wire (FW) electrodes.

The objective of our study is to apply the time-frequency distribution to the EMG signal during muscle fatigue. The EMG signals were collected using surface electrode. Figure 18 shows a mesh plot of the EMG signal during muscle fatigue using the smoothed pseudo Wigner distribution. In this calculation, the length of analysis window, length of FFT and the skip points were 0.0423 second, 256 points and 100 points respectively.

Looking at figure 18, we observe that as time goes from zero to 30 seconds, the range of frequencies with significant power is declining and power density increases. This is in agreement with the result of standard FFT spectral analysis during muscle fatigue. Thus, we obtained the same conclusion (declination of frequency during muscle fatigue) by looking at the mesh plot of the time-frequency distribution.

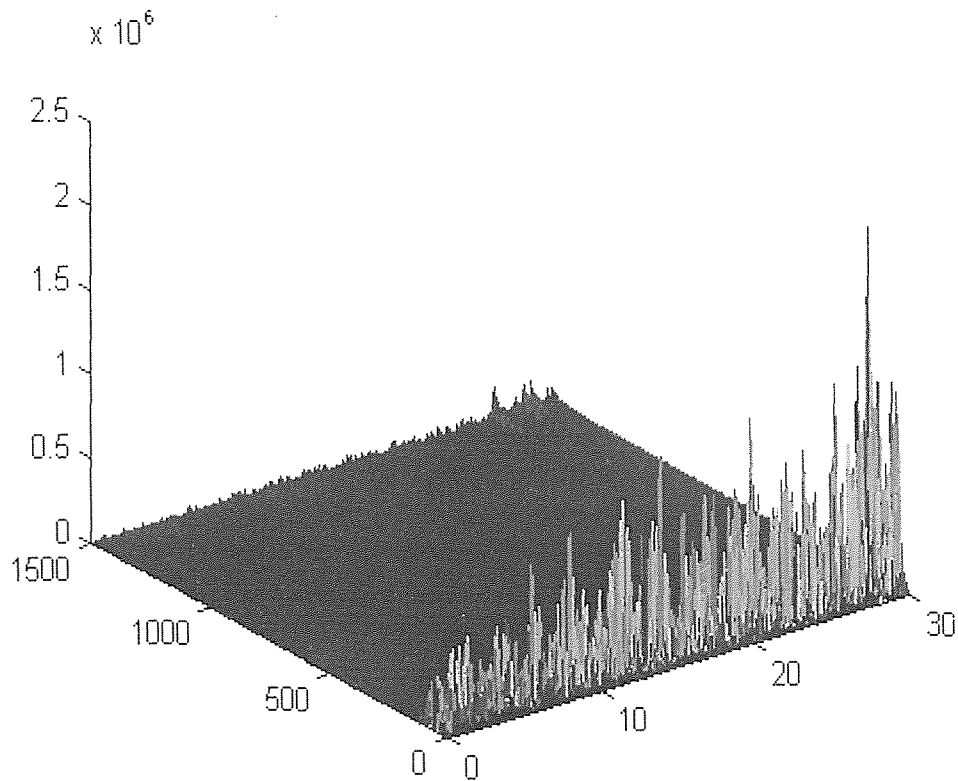


Figure 18 The mesh plot of EMG signal during muscle fatigue

The median frequency was calculated for each time slice (length of 0.0423 second). The variable analyzed was the slope of a regression line, fit to the median frequencies. To establish reliability between the median frequency and the regression line, we also calculated the correlation coefficient. Figure 19 superimposes the median frequency and the regression line.

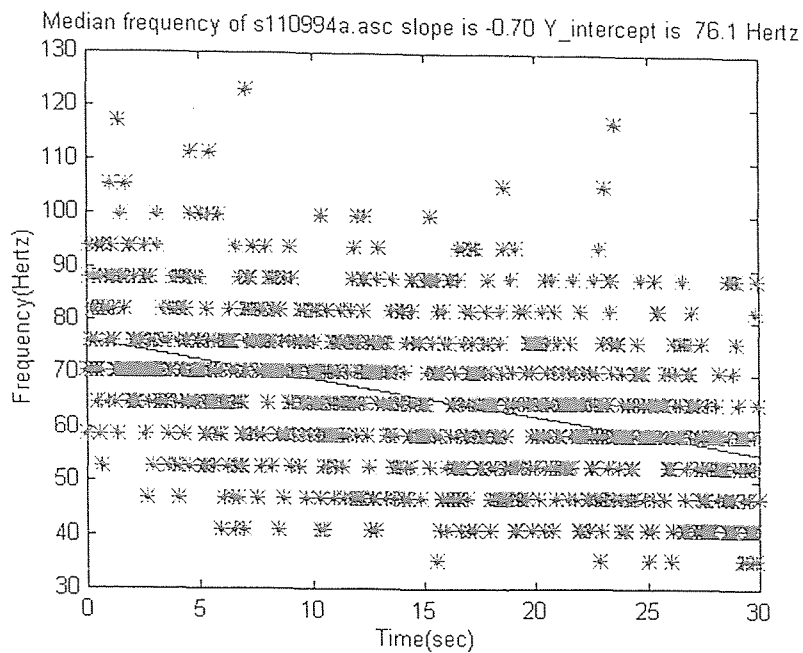


Figure 19 The above plots are calculated from the EMG signal using surface electrodes. The variables are as follow Lwin=127; FFTlen=256; skip=100; rcoef=-0.4

The slope of the regression line, the initial median frequency and the correlation coefficient recorded as -0.7, 76.1(hertz) and -0.4 respectively. The negativity of the slope is acceptable since the median frequency decays with fatigue. The correlation coefficient was very small because the length of the analysis window was very small. Thus, taking the length of analysis window small(0.0423 sec), it gives us very good time resolution (0.033 sec) but poor correlation coefficient(-0.4).

In the next case, we applied the SPWD to the same data file(the EMG signal during muscle fatigue using surface electrode), but we increased the length of the analysis window to 0.17 second , the FFT length of 512 and kept the skip point same as before(100). Figure 20 superimposes the median frequency and the regression line.

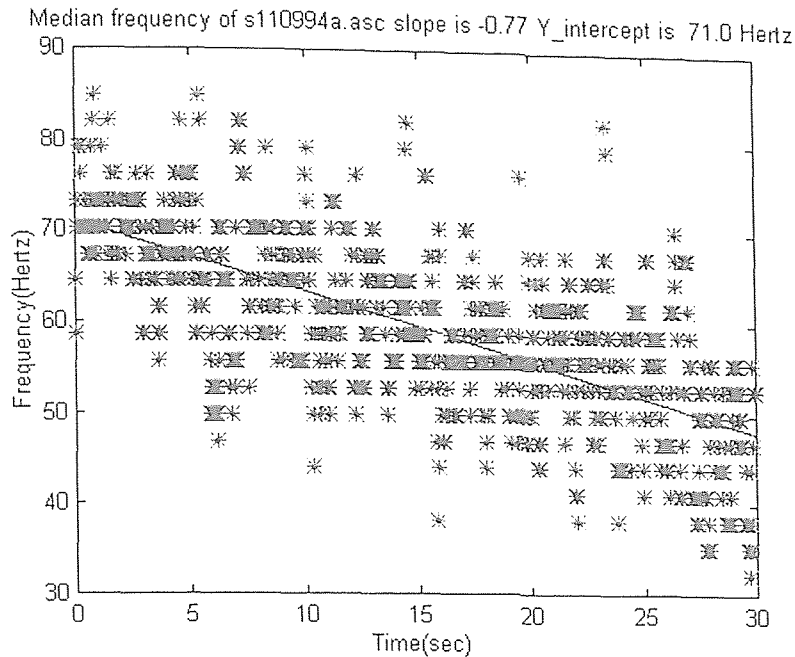


Figure 20 The above plots are calculated from the EMG signal using surface electrodes. The variables are as follow:
Lwin=511; FFTlen=512; skip=100; rcoef=-0.7

We recorded the slope of the regression line, the initial median frequency and the correlation coefficient as -0.77, 71(hertz) and -0.7 respectively. The negativity of the slope is acceptable as we explained before(the median frequency decays with fatigue). The initial median frequency decreased and the correlation coefficient decreased, since we used larger analysis window but still correlation coefficient of -0.7 is low. Table 5 shows the statistical value from the smoothed Wigner distribution for surface to surface electrode.

Table 5 Results from SPWD of EMG using surface electrode

surface to surface electrode	length of analysis window	FFT length	skip point	slope	initial median frequency	correlation coefficient
trial #1	127	256	100	-0.7	76.1	-0.4
trial #2	511	512	100	-0.77	71.0	-0.7

We also applied the smoothed pseudo Wigner distribution to the EMG signal during muscle fatigue, using fine wire electrodes. To compare the fine wire electrodes with the surface electrodes, we used the length of analysis window, length of FFT and the skip point to be 0.0423 second, 256 points and 100 points respectively. Figure 21 superimposes the median frequency and the regression line in case of the fine wire electrode.

we also computed the slope of the regression line, the correlation coefficient and the initial median frequency for fine wire electrodes. The slope of the regression line, the initial median frequency and the correlation coefficient recorded as -0.83, 125.8(hertz) and -0.4 respectively. The negativity of the slope is acceptable since the median frequency decays with fatigue. The correlation coefficient was very small because the length of the analysis window was very small.

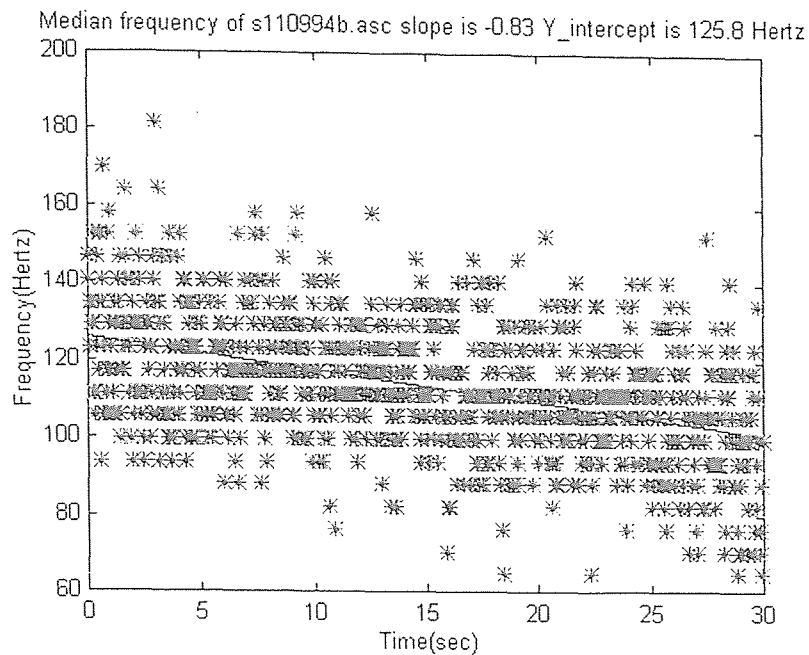


Figure 21 The above plot is calculated from the EMG signal using fine wire electrodes. The variables are as follow:
 $Lwin=127$; $FFTlen=256$; $skip=100$; $rcoef=-0.4$

Next, we applied the SPWD to the same data file(the EMG signal during muscle fatigue using fine wire electrodes), but we increased the length of the analysis window to 0.17 second , the FFT length of 512 and kept the skip point same as before(100). Figure 22 superimposes the median frequency and the regression line.

We recorded the slope of the regression line, the initial median frequency and the correlation coefficient as -0.74, 120.3(hertz) and -0.62 respectively. The initial median frequency decreased and the correlation coefficient improved, since we used larger analysis window but still correlation coefficient of -0.62 is very low. Table 6 shows the statistical value from the smoothed Wigner distribution for fine wire electrode.

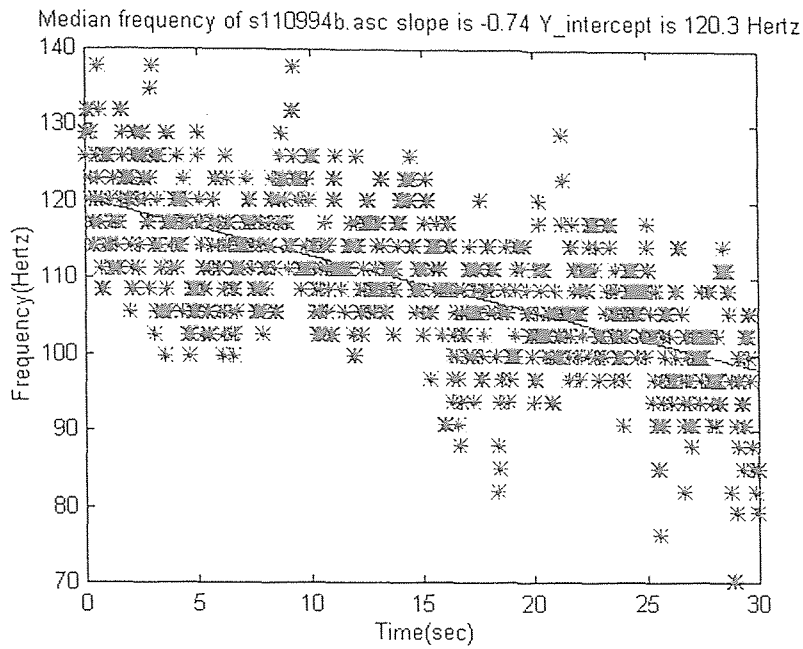


Figure 22 The above plot is calculated from the EMG signal using fine wire electrodes. The variables are as follow:
 $L_{win}=511$; $FFT_{len}=512$; $skip=100$; $r_{coef}=-0.62$

The results from the time-frequency distribution were compared with the work(spectral FFT analysis) of Maniar[15]. Table 7 shows the statistical values from Maniar's work.

Table 6 Results from SPWD of EMG using fine wire electrode

fine wire electrode	length of analysis window	FFT length	skip point	slope	initial median frequency	correlation coefficient
trial #1	127	256	100	-0.83	125.8	-0.4
trial #2	511	512	100	-0.74	120.3	-0.62

In the case of surface to surface electrode, we used the results from trial #2 to compare with Maniar's work[15]. The slope's are both negative, but the magnitudes are very different.

The initial median frequencies are very close but not exact. The correlation coefficient from Maniar's work is close to -1, which is the desirable coefficient. The time-frequency distribution method showed poor correlation coefficient(-0.77).

Table 7 The Statistical Values from Maniar's Work

	Surface to surface electrode	fine wire electrode
slope	-1.810	-1.473
initial median frequency	69.110	117.687
correlation coefficient	-0.958	-0.925

In the case of fine wire electrode, we also used the results from trial #2 to compare with Maniar's work. The time-frequency distribution showed poor correlation coefficient. the magnitudes of slope are very different. The initial median frequencies are close but not exact. Since the correlation coefficients were very low, we did not compare the surface to surface electrode with fine wire electrode.

As can be seen, results from the spectral analysis and the time-frequency distribution were different. but, as we increased the length of analysis window the correlation coefficient improved . More work has to be done on time-frequency distribution before one can deny the capability of time-frequency analysis in case of the EMG signal during muscle fatigue.

CHAPTER 5

CONCLUSION

5.1 Development of the Time-Frequency Signal Analysis Toolbox

We have developed a time-frequency signal analysis toolbox. The original computer algorithm(FORTRAN CODE) of time-frequency representation was presented by Boashash[1]. In this research we have regenerated his algorithm which implement time-frequency signal analysis techniques on the Matlab software. Its primary function is to produce a variety of time-frequency representations and plots from the time series. Time-frequency distributions (TFDs) are powerful tools for the analysis and processing of nonstationary signals for which separate time-domain and frequency-domain analysis are not adequate. In this thesis, we have outlined the motivations, interpretations, mathematical fundamentals, properties, and applications of various linear and quadratic TFDs. Although we have attempted to provide a coherent framework of TFDs, a truly unified framework is difficult to obtain because of the large variety of existing methods and approaches causing the field of time-frequency analysis to be somewhat disparate. We showed the trade off between time and frequency resolution in case of the short-time Fourier transform. The resolution of the Wigner distribution was relatively poor, in spite of high auto component concentration. The pseudo Wigner distribution and the smoothed pseudo Wigner distribution all require a careful choice of the window, with the resolution dependent on that choice. The smoothed pseudo Wigner distribution contained many

good properties of the Wigner distribution. Among all the distribution, we decided to use the smoothed pseudo Wigner distribution (SPWD) for our further research, because it suppressed the cross terms and for certain types of smoothing, a positive distribution is obtained. The advantage of the Choi-Williams distribution was that it is insensitive to the signal component scaling, so an acceptable smoothing parameter can be chosen independently of the data. The Born-Jordan distribution has been introduced, which have many desirable properties. It has been shown that this new distribution provides a high resolution, easy to interpret localization of the signal energy spectrum in the time-frequency plane. A systematic procedure to design the new kernels has been introduced.

5.2 Biomedical Application of Time-Frequency Distribution

5.2.1 Sympatho-vagal balance

The utilization of time-frequency analysis is vast. Calculation of sympatho-vagal balance from the time-frequency distribution describes the changes of the parasympathetic and sympathetic influences on heart rate. Time-frequency calculation of the sympatho-vagal balance recognized the reciprocal parasympathetic and sympathetic influences on heart rate, through the ratio of low frequency power to high frequency power. The time-frequency calculation of the sympatho-vagal balance indicated how this ratio changed as a function of time. The time-frequency presentation indicated that, detrending the IBI signal can remove information at low frequencies.

5.2.2 Time-Frequency Distribution of EMG Signal

Utilizing the time-frequency distribution, we compared median frequency and decline in median frequency for the EMG signal during muscle fatigue with the spectral analysis method. The time-frequency distribution result showed decline of the median frequency during muscle fatigue. We obtained very poor correlation coefficient via time-frequency distribution, but as we increased the length of analysis window the correlation coefficient improved. The results from the spectral analysis and the time-frequency distribution were different and the comparison failed due to very poor correlation coefficient.

APPENDIX A

For our purpose, part of the main source code is presented at this point and number each line for further explanation.

```

1. for K=1:Timeslice,
2. for m=0:hlf,
3. R(m+1)=G(l,m+1)*z(l+m+n)*conj(z(l-m+n));
4. for P=1:hlf,
5. R(m+1)=R(m+1)+(G(P+1,m+1)*((z(l+P+m+n)*conj(z(l+P-m+n)))+(z(l-P+m+n)*conj(z(l-P-
m+n)))));
6. if m>0, R(ffilen-m+1)=conj(R(m+1)); end
7. end
8. end
9. for m=hlf+2:ffilen-hlf, R(m)=0; end
10. tfds=2/ffilen*abs(ffl(R));
11. TFDs(:,K)=tfds(1:ffilen)';
12. n=n+skip
13. end

```

where description of variables are as follows:

- $z(\)$ is an analytic input signal.
- $conj(z(\))$ is complex conjugate of the input signal.
- $G(\)$ is selection kernel matrix.
- $R(\)$ is matrix where result of convolution is stored.
- l indicate the center of the analysis window.
- $skip$ the number of time samples to skip between successive slices of analysis
- $TFDs$ is matrix where the result of TFD is stored.
- $Timeslice$ indicates the number of time slice.
- m and p are lower and upper indexes of summation.

In the code fragment shown above (line 2-5), the symmetry is used by multiplying the

$G(n, m)$ value with the required two bilinear product values at the same time, for a signal window of length $2 \times hlf + 1$. On line 6, we take advantage of symmetry of $G(n, m)$ and the corresponding kernel product to compute the upper half of the result matrix $R()$ from the lower half through conjugation. On line 9 we are adding sufficient number of zeros to matrix $R()$, called zero padding, before taking the discrete Fourier transform each time. This is due to restrictions in the fast-Fourier transform routine (FFT) on the length of each data segment (usually to a power of two). This way any points containing calculated values are set to zero, as the FFT length may be greater than the analysis window. On line 10-11 we compute the power spectral density of each time slice and place them by order into the matrix $TFDs$ respectively.

Variable hlf determine the size of the kernel and bilinear product for analysis. It is defined as:

$$hlf = \frac{Lwin + 1}{2} - 1$$

where $Lwin$ is the size of the analysis window and must be odd. Variable $skip$ determines the number of time samples to skip between successive slices of the analysis window and dividing the $skip$ by the sampling frequency of input signal gives us the time resolution. The presence of index $1 (= 2 \times hlf + 1)$ as the center of the analysis window guarantees the nonnegativity of indices into the signal $z()$ since the Matlab compiler generates code to check array bounds for negativity.

The following are typical questions and respond which user has to understand.

- *Please enter the name of datafile with no extension.*

The user has to make sure that the extension of the datafile is “.asc”, and the datafile contains ASCII data in a columnwise fashion.

- *Which column do you want to analyze.*

If the user’s datafile contains many columns of data, the user should indicate which column s/he wants to analyze. i.e., <1>, <2>, ...

- *Please enter the length of analysis window.*

The user has the option to pick the size of analysis window (odd number), as described in the previous section.

- *Please enter the length of FFT analysis.*

The user can enter a number equal to or greater than the length of the analysis window.

Note if the number is a power of 2, Matlab uses one of the fast discrete Fourier transform routines, otherwise Matlab uses a non power of two algorithm. Note, if the length of FFT is greater than analysis window then zero padding is applied.

- *Please enter the number of the skip points.*

The number of skip determines the time resolution. Usually this number should be smaller than the length of analysis window.

$$\text{time resolution} = \frac{\text{skip points}}{\text{sampling frequency of signal}}$$

$$f_{\text{resolution}} = \frac{f_{\text{sampling}}}{2 * \text{FFTlength}}$$

The number “2” is due to the analytical signal.

- *Please enter the sample rate of the data.*

The user should enter the sampling frequency of datafile.

- *Do you want to detrend the input signal.*

If the user answers yes, then the user will be asked to enter the order of the low pass filter and the cutoff frequency.

- *Do you want to calculate instantaneous frequency.*

The user has the option to enter yes <y>, or no <n>

- *Do you want to calculate median frequency.*

If the user answers yes, then the user will be asked to enter the low and high frequencies (frequency band of interest in hertz).

- *Do you want to extract certain frequency range.*

If the user answers yes, then the user will be asked to enter the low and high frequency of interest in terms of the index. In order to calculate index values divide the desired frequency by the frequency resolution.

- *Do you want to look at, a)mesh&contour b)mesh c) contour d)none*

The user can choose the plotting method.

```

%                               signal.m
%
%                               This is the source code for creating three different
%                               signals, which each signal is made of three sine wave
%                               with frequencies of 2 , 5 and 10 hertz.
%                               the sampling frequency for the all signals is 100
%                               samples per second.
%                               Each signal is located as a one column of matrix
%                               sig_tes. The length of FFT is 2048 points.
%                               The plots of power spectrum are zoomed in.
%                               The last two line of the instructions is used to
%                               save the figures in Metafile format and then
%                               is imported to Microsoft word (ver, 6.0a).
t=0:0.01:1.99;
signal_1=[zeros(1,50) sin(2*pi*5*t) zeros(1,50) sin(2*pi*2*t) zeros(1,100)
sin(2*pi*10*t)]';
signal_2=[zeros(1,50) sin(2*pi*10*t) zeros(1,50) sin(2*pi*5*t) zeros(1,100)
sin(2*pi*2*t)]';
signal_3=[sin(2*pi*2*t) zeros(1,100) sin(2*pi*10*t) zeros(1,100) sin(2*pi*5*t)]';
sig_tes=[signal_1 signal_2 signal_3];
ref=length(signal_1);
Pyy=abs(fft(sig_tes,2048));
F=(100*(0:511)/2048)';
T=(ref/100)/(ref-1)*(0:ref-1);
figure(1);
subplot(3,1,1), plot(T,signal_1); xlabel('Time(second)'); ylabel('Amplitude');
subplot(3,1,2), plot(T,signal_2); xlabel('Time(second)'); ylabel('Amplitude');
subplot(3,1,3), plot(T,signal_3); xlabel('Time(second)'); ylabel('Amplitude');
pause
figure(2);
subplot(3,1,1), plot(F,Pyy(1:512,1)); xlabel('Frequency(hertz)'); ylabel('Power Density');
subplot(3,1,2), plot(F,Pyy(1:512,2)); xlabel('Frequency(hertz)'); ylabel('Power Density');
subplot(3,1,3), plot(F,Pyy(1:512,3)); xlabel('Frequency(hertz)'); ylabel('Power Density');
print -dmeta -ffigure(1) sine.cgm;
print -dmeta -ffigure(2) sin_fft.cgm;

```

```

%                               Sine.m
%                               This is the source code for generating the
%                               data file for the PWD cross term and Choi-Williams illustration
clear
close("all")
t=0:0.001:4; x=(sin(2*pi*100*t)+sin(2*pi*400*t))'; ref=length(x);
T=(ref/100)/(ref-1)*(0:ref-1); plot(T,x); save sine1.asc x -ascii

```

The following program written in Matlab was utilized to perform Time-Frequency analysis.

```

%                               TFD.m
%       This the source code for utilizing the time-frequency representation.
%       User should refer to the beginning of this appendix for further instruction to
%       operate this software.

close('all')
clear
clc
choose=menu('SELECT YOUR DISTRIBUTION','SPWD',...
            'Choi_Williams','Spectrogram',...
            'Born_Jordan_Cohen (RID)','Rihaczek_Margenau','PWD');
clc
disp("")
disp([blanks(30) 'WELLCOME TO'])
disp([blanks(21) 'TIME FREQUENCY DISTRIBUTION'])
disp([blanks(33) 'WORLD'])
disp("")
disp("")
SIGNAL=input('Please enter name of datafile with no extension --> ','s');
filename=[SIGNAL,'.asc'];
eval(['load ' filename]);
original_rawdata=eval(SIGNAL);
clear eval(SIGNAL) s110994b;
Question_1=input('Which column do you want to analyze? [1 2 3] --> ','s');
if      Question_1=='1'
    rawdata=original_rawdata(1,:);
elseif Question_1=='2'
    rawdata=original_rawdata(2,:);
elseif Question_1=='3'
    rawdata=original_rawdata(3,:);
end
clear original_rawdata;
Signa=rawdata;
%
Lwin=input('Please enter the length of analysis window --> ');
fftlen=input('Please enter the length of FFT analysis --> ');
skip=input('Please enter the number of the skip points --> ');
sample=input('Please enter the sample rate of the data --> ');
Question_2=input('Do you want to deterend the input signal? [y/n] --> ','s');
if Question_2=='y'
    order=input('Please enter the order of the lowpass filter --> ');
    freq=input('Please enter the cutoff frequency for LPF --> ');

```

```

    nfreq=freq/sample;
    [poles,zero]=butter(order,nfreq);
    dtrend=filtfilt(poles,zero,rawdata);
    Result_Signa=rawdata-dtrend;
    Signa=Result_Signa;
else
end
Question_3=input('Do you want to calculate Instantaneous Frequency? [y/n] --> ','s');
Question_4=input('Do you want to calculate Median Frequency? [y/n] --> ','s');
if Question_4=='y'
    LF=input('Please enter the low frequency? [Hz] -->');
    HF=input('Please enter the High frequency? [Hz] -->');
else
end
Question_6=input('Do you want to extract certain Frequency range? [y/n] --> ','s');
if Question_6=='y';
    LFC=input('Please enter the low frequency range in index -->');
    HFC=input('Please enter the high frequency range in index -->');
else
end
hlf=(Lwin+1)/2-1;
I=2*hlf+1;
signal=hilbert([zeros(1,2*hlf) Signa zeros(1,2*hlf)]);
signal_conjugate=conj(signal);
%
%           (Smoothed WVD using a rectangular window of odd length)
%
if choose==1
P=input('Please enter the length of smoothing region --> ');
distribution=['Smoothed WVD'];
G=(1/(2*P-1))*ones(hlf+1,hlf+1);
smoothing_region=ones(hlf+1,hlf-P+1);
G(:,P+1:hlf+1)=zeros(size(smoothing_region));
%
%           (Choi-Williams)
%
elseif choose==2
distribution=['Choi_Williams'];
Sigma=0.1;
G=zeros(hlf+1,hlf+1); G(1,1)=1.0;
for j=1:hlf;
for i=0:hlf, G(i+1,j+1)=exp((((-1)*Sigma*i*i)/(4*j*j)); end
G(:,j+1)=G(:,j+1)/(2*sum(G(:,j+1))- G(1,j+1));
end
%           (Spectrogram)

```



```

%
elseif choose==3
distribution=['Spectrogram'];
G=(1/(2*hlf-1))*fliplr(triu(ones(hlf+1,hlf+1),0));
%
%                               (Born-Jordan-Cohen)
%
elseif choose==4
distribution=['Born_Jordan_Cohen'];
G=triu(ones(hlf+1,hlf+1),0);
for i=0:hlf, G(i+1,:)=(1/(1+i))*G(i+1,:);
end
%
%                               (Rihaczek-Margenau)
%
elseif choose==5
distribution=['Rihaczek_Margenau'];
G=ones(hlf+1,hlf+1);
G=0.5*diag(diag(G));
G(1,1)=1;
end
%
%                               (Computation of TFDs)
%
Timeslice=floor((length(signal)-4*hlf-1)/skip);
kernel=zeros(fftlen,Timeslice);
TFDs=zeros(Lwin,Timeslice);
if Timeslice<=0
disp(' ')
disp('---> The size of data file is less than the length of FFT');
disp('---> Therefor the process will be terminate now. ');
disp('---> Please reduce the length of FFT and try again. ');
break;
end
h = waitbar(0,'Please wait while it is processing...');
if choose<6
for n=0:skip:skip*(Timeslice-1);
for m=0:hlf,
kernel(m+1,(n/skip)+1)=(G(1,m+1)*signal(I+m+n)*signal_conjugate(I-m+n))...
+sum(G(2:hlf+1,m+1).*(signal(I+1+m+n:I+hlf+m+n).*signal_conjugate(I+1-m+n:I+hlf-
m+n))...
+signal(I-1+m+n:-1:I-hlf+m+n).*signal_conjugate(I-1-m+n:-1:I-hlf-m+n));
end
waitbar(n/(length(signal)-4*hlf-1))
end
clear signal_conjugate signal
kernel(fftlen-hlf+1:fftlen,:)=flipud(conj(kernel(2:hlf+1,:)));
TFDs=2/fftlen*abs(fft(kernel,fftlen));

```

```

close(h)
else
distribution=['PWD'];
for n=0:skip:skip*(Timeslice-1);
V1=signal(I+n:I+hlf+n).*signal_conjugate(I+n:-1:I-hlf+n);
kernel(1:hlf+1,(n/skip)+1)=(V1+sqrt(-1)*V1)';
kernel(fftlen:-1:fftlen-hlf+1,(n/skip)+1)=((sqrt(-
1)*conj(V1(2:hlf+1)))+(imag(V1(2:hlf+1))+(real(V1(2:hlf+1))*sqrt(-1)))));
waitbar(n/(length(signal)-4*hlf-1))
end
kernel=flipud(kernel);
TFDs=2/fftlen*abs(fft(kernel));
close(h)
end
clear signal kernel signal_conjugate;
%
%           (Algorithem to calculate instantaneous frequency)
%
if Question_3=='y';
[r,C]=size(TFDs);
for i=1:C,
W=TFDs(:,i);
Y=(1:r)';
M=W.*Y;
S=sum(M);
F=sum(W);
E(i)=S/F;
end
elseif Question_3=='n';
end
end
%
%           (Algorithem to extract certain frequency)
%
if Question_6=='y';
symvag=sum(TFDs(LFC,1:Timeslice));
vagal=sum(TFDs(HFC,1:Timeslice));
symtopar=symvag./vagal;
end
elseif Question_6=='n';
end
%
%           (Three Dimensional Graphics)
%
T=(length(Signa)/sample)/(Timeslice)*(0:Timeslice-1);
f=(sample/(2*fftlen))*(0:fftlen-1);

```

```

c=length(Signa);
ref=(c/sample)/(c-1)*(0:c-1);
%
if Question_4=='y';
    low=1;
    while f(low)<LF
        low=low+1;
    end
low_freq=low;
    high=fftlens/2+1;
    while f(high)>HF
        high=high-1;
    end
high_freq=high;
    lo_hi=low_freq:high_freq;
    desire_median_power=sum(TFDs(lo_hi,:))/2;
    [ROW,COL]=size(TFDs);
    median_frequency=zeros(1,COL);
for slice_power=1:COL
    col_index=low_freq;
    Median_Power=TFDs(low_freq,slice_power);
    while Median_Power < desire_median_power(slice_power)
        col_index=col_index+1;
        Median_Power=Median_Power+TFDs(col_index,slice_power);
    end
    median_frequency(slice_power)=f(col_index);
end
%
%           (Algorithem to Line fit the Median frequency)
%
    feeding=polyfit(T,median_frequency,1);
    fit=polyval(feeding,T);
elseif Question_4=='n';
end
disp('Do you want to look at (a)mesh&Contor , (b)mesh')
disp(['blanks(24) '(c)contour, (d)None'])
FigType=input('-->','s');
if FigType=='a';
    figure(1); subplot(2,1,1), mesh(T,f,TFDs);
    xlabel('Time(sec)'); ylabel('Frequency(hertz)'); zlabel('Magnitude');
    title(['Mesh & Contour of ',eval('filename'),' using ',eval('distribution'),' distribution']);
    subplot(2,1,2), contour(T,f,TFDs); xlabel('Time(sec)'); ylabel('Frequency(Hz)');
pause
elseif FigType=='b';
    figure(1); mesh(T,f,TFDs);
    xlabel('Time(sec)'); ylabel('Frequency(Hz)'); zlabel('Magnitude');

```

```

    title(['Mesh of ',eval('filename'),' using ',eval('distribution'),' distribution']);
pause
elseif FigType=='c';
    figure(1); contour(T,f,TFDs);
    xlabel('Time(sec)'); ylabel('Frequency(hertz)');
    title(['Contour of ','sine.asc',' using ',eval('distribution'),' distribution']);
pause
elseif FigType=='d';
end
%           (Algorithem to calculate Median frequency)
%
if Question_4=='y';
slope=(fit(3)-fit(1))/(T(3)-T(1));
S1 = sprintf('slope is %5.2f,(fit(3)-fit(1))/(T(3)-T(1));');
S2 = sprintf('Y_intercept is %5.1f,fit(2)-slope*T(2));');
COEF=corrcoef([median_frequency fit]);
rcoef=COEF(1,2);
figure(2);
plot(T,fit,T,median_frequency,'*');
title(['Median frequency of ',eval('filename'),' ',eval('S1'),' ',eval('S2'),' ',Hertz]);
xlabel('Time(sec)'); ylabel('Frequency(Hertz)');
else
end
pause
if Question_3=='y' & Question_2=='y';
    figure(3);
    subplot(3,1,1), plot(ref,rawdata);
    title(['Superimpose of rawdata & detrended & IF of ',eval('filename')]);
    xlabel('Time(sec)'); ylabel('Amplitude'); subplot(3,1,2),plot(ref,Signa);
    xlabel('Time(sec)'); ylabel('Amplitude'); subplot(3,1,3), plot(T,E);
    xlabel('Time(sec)'); ylabel('frequency');
elseif Question_3=='y' & Question_2=='n'
    figure(3);
    subplot(2,1,1), plot(ref,rawdata);
    title(['Superimpose of rawdata of ',eval('filename'),' & IF']);
    xlabel('Time(sec)'); ylabel('Amplitude'); subplot(2,1,2),plot(T,E);
    xlabel('Time(sec)'); ylabel('Amplitude');
elseif Question_3=='n' & Question_2=='y'
    figure(3);
    subplot(2,1,1), plot(ref,Signa);
    title(['plot of rawdata & detrended of ',eval('filename')]);
    xlabel('Time(sec)'); ylabel('Amplitude'); subplot(2,1,2),plot(ref,Signa);
    xlabel('Time(sec)'); ylabel('Amplitude');
elseif Question_3=='n' & Question_2=='n'
    figure(3);

```

```
plot(ref,Signa); title(['plot of rawdata of ',eval('filename')]);
xlabel('Time(sec)');ylabel('Amplitude');
end
pause
if Question_6=='y';
    figure(4);
    subplot(3,1,1), plot(T,symvag);
    title(['Mixture of Sym&Parasym & Parasym range & Ratio of Lowfreq to HighFreq']);
    xlabel('Time(sec)'); ylabel('Amplitude');
    subplot(3,1,2), plot(T,vagal);
    xlabel('Time(sec)'); ylabel('Amplitude');
    subplot(3,1,3), plot(T,symtopar);
    xlabel('Time(sec)'); ylabel('Amplitude');
if Question_6=='n';
end
end
```

REFERENCES

- [1] B. Boashash. *Time-Frequency Signal Analysis Methods and Applications*, Wiley Halsted Press, 8-42, 1992.
- [2] L. Cohen, "Time-Frequency Distributions - A Review", Proceedings of the IEEE, Vol. 77, No. 7, July 1989.
- [3] F. Hlawatsch and G. F. Boudreaux-Bartels. "Linear and Quadratic Time-Frequency Signal Representations", IEEE SP Magazine, 21-67, April 1992.
- [4] R. E. Ziemer and W. H. Tranter. *Principles of Communications*. Houghton Mifflin Company. Third Edition, 19-119, 1990.
- [5] E. Kreyszig. *Advanced Engineering Mathematics*, John Wiley and Sons, Inc. Seventh Edition. 392-414, 1993.
- [6] P. V. O'Neil. *Advanced Engineering Mathematics*, Wadsworth Publishing Company. Second Edition. 575-585, 1987.
- [7] W. Chase, F. Bown. *General Statistics*, John Wiley and Sons, Inc. Second Edition. 460-496, 1992.
- [8] R. A. Normann. *Principles of Bioinstrumentation*, John Wiley and Sons, Inc. 168-170, 1988.
- [9] J. Jeong and W. J. Williams. "Kernel Design for Reduced Interference Distributions", IEEE Transactions on Signal Processing, Vol. 40, No. 2, February 1992.
- [10] D. L. Jones and T. W. Parks. "A Resolution Comparison of Several Time-Frequency Representations", IEEE Transactions on Signal Processing, Vol. 40, No. 2, February 1992.
- [11] T.A.C.M. Classen and W.F.G. Mecklenbrauker. "The Wigner Distribution-a Tool for Time-Frequency Signal Analysis", Philips J. Res. 35, Part I, 217-250; Part II, 276-300; Part III, 372-389, 1980.
- [12] N. Yen. "Time and Frequency Representation of Acoustic Signals by Means of the Wigner Distribution function: Implementation and Interpretation", J. Acoust. Soc. Am. 81(6), 1841-1850, June 1987.
- [13] M. Amin, L. Cohn and W.J. Williams. "Methods and Applications for Time-Frequency Analysis" Conference Notes, University of Michigan, 1993.

- [14] R. M. Davies. "Time Frequency Analysis of Electromyogram During Muscle Fatigue", NJIT, MS Thesis, January 1994.
- [15] R. M. Maniar. "Time domain and Frequency Domain Analysis of Myoelectric Signals During Muscle Fatigue", NJIT, MS Thesis, January 1995.
- [16] S. Fernando. "Autonomic Nervous System Evaluation using Time-Frequency Analysis", NJIT, MS Thesis, October 1994.
- [18] Matlab. *High-Performance Numeric Computation and Visualization Software*, Reference Guide, The Math Works, Inc. August 1992.
- [19] K. H. Wesseling, J. J. Settles and B. deWit, The Measurement of Continuous Finger Arterial Blood Pressure Non-invasively in Stationary Subjects. In: *Biological and Psychological Factors in Cardiovascular Disease*. T. H. Schmidt, T. M. Dembroski and G. Blumchen, 355-375, 1986.
- [20] M. T. LaRovere, G. Speechia, A. Mortara and P. J. Schwartz. "Baroreflex Sensitivity, Clinical Correlates, and Cardiovascular Mortality Among Patients with a First Time Myocardial Infarction", *Circulation*, 78(4), 816-824, 1988.
- [21] R. A. Nishimura and A. J. Tajik. "Cardiovascular Clinics: The Valsalva Maneuver and Response Revisited". *Mayo Clin Proc*, 61:211-217, 1986.
- [22] E.I. Elisberg. "Heart Rate Response to the Valsalva Maneuver as a Test of Circulatory Integrity". *JAMA*, 120-186, 1973.
- [23] B. Pomeranz, R. J. B. Macaulay, M. A. Kutz, I. Adam, D. Gordon, D. Kilborn, K. M. Barger, A. C. Shannon, D. C. Cohen, R. J. Cohen and H. Benson. "Assessment of Autonomic Function in Humans by Heart Rate Spectral Analysis". *Am. J. Physiol*, 248, H151-3, 1985.
- [24] C. H. Hockman. "Essentials of Autonomic Function", IL, Springfield, 1987.
- [25] R. Furlan, S. Guzzetti, W. Crivellaro, S. Dassi, M. Tinelli, G. Baselli, S. Cerutti, F. Lombardi, M. Pagani and A. Malliani. "Continuous 24-hour assessment of the neural regulation of systemic arterial pressure and RR variabilities in ambulant subjects". *Circulation* 81, 537-47, 1990.
- [26] W. H. J. P. Linssen, D. F. Stegememan, E. M. G. Joosten, M. A. Van'tHof, R. A. Binkhorst and S. L. H. Notermans. "Variability and Interrelationships of Surface EMG Parameters During Local Muscle Fatigue". *Muscle and Nerve*, 849-856, 1993.

- [27] E. Kwatny, D. H. Thomas and H. G. Kwatny. "An Application of Signal Processing Techniques to the Study of Myoelectric Signals". IEEE Trans Biomed Eng 17(4), 303-311, 1970.
- [28] C. Krog-Lund and K. Jergensen. "Myo-electric Fatigue Manifestations Revisited: Power Spectrum, Conduction Velocity and Amplitude of Elbow Flexor Muscles During Isolated and Repetitive Endurance Contractions at 30% Maximal Voluntary Contraction". Eur. J. Appli Physiol 66, 161-173, 1993.